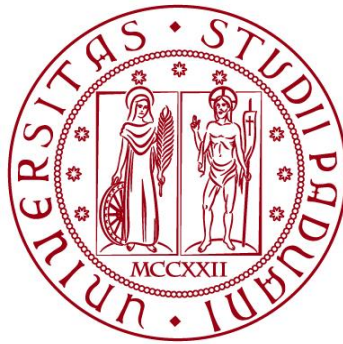


UNIVERSITÀ DEGLI STUDI DI PADOVA

DIPARTIMENTO DI BIOLOGIA

Corso di Laurea magistrale in Marine Biology



TESI DI LAUREA

**Physiological Responses of *Ulva* sp. to
Heatwaves**

Relatore: Prof.ssa Isabella Moro
Dipartimento di Biologia

Correlatore: Dr. João Miguel Sousa da Silva
Centre of Marine Sciences (CCMAR)

Laureanda: Marta Paganin

ANNO ACCADEMICO 2023/2024

Abstract

Marine heatwaves (MHWs) are becoming increasingly frequent due to climate change, significantly impacting marine ecosystems, including macroalgae such as *Ulva* spp. This study aims to investigate the physiological responses of *Ulva* sp. to simulated heatwave conditions. Algal samples were exposed to three thermal regimes: a single heatwave (SH), two consecutive heatwaves (DH), and a control condition without thermal stress. The heatwave simulation involved raising the water temperature from 18°C to 24°C for 7 days, followed by a 7-day recovery period at 18°C. Physiological changes were assessed by measuring pigment, protein, sugar, and starch levels, along with photosynthetic performance through photosynthesis-irradiance (PI) curves.

The analysis of photosynthetic parameters and biomolecule levels revealed clear physiological responses to thermal stress. Both SH and DH treatments showed a significant increase in photosynthetic activity (P_{max}) during peak heatwave phases and recovery periods, though the response differed between treatments. The DH treatment displayed higher P_{max} during the initial recovery phase (T2) and at the second heatwave peak (T3), suggesting possible adaptive responses such as increased photosynthetic pigment synthesis and enhanced energy allocation for cellular repair. Furthermore, increases in chlorophyll-a and carotenoid levels in the DH treatment indicated that *Ulva* sp. may use pigments for enhanced light capture and antioxidant protection under stress. Protein levels also rose in DH, suggesting a synthesis of structural and stress-response proteins that maintain cellular integrity under repeated heat exposure.

Overall, *Ulva* sp. demonstrated physiological plasticity in response to thermal stress, suggesting potential resilience to future warming events. The findings contribute valuable insights into the adaptive capacity of macroalgae, with implications for

the conservation and restoration of marine ecosystems facing
climate-induced thermal stress.

Table of Contents

1. Introduction	1
1.1 Marine Heatwaves: their Intensification Linked to Climate Change and Effects on Marine Biodiversity	1
1.2 <i>Ulva</i> spp. and their Ecological Role	5
1.3 Influence of MHWs on Algal Communities and the Role of Thermal Priming	6
1.4 Main objectives.....	8
2. Materials and methods	8
2.1 Study site	8
2.2 Experimental design	11
2.2.1 <i>Ulva</i> sp. collection.....	11
2.2.2 Mesocosm experiment setup.....	11
2.2.3 Experimental and sampling design	13
2.3 Photosynthetic activity : Photosynthesis-Irradiance (P-I) response curve....	14
2.4 Biochemical Composition	17
2.4.1 Protein extraction and quantification	18
2.4.2 Photosynthetic Pigment Extraction and Quantification	19
2.4.3 Non-Structural Carbohydrates Quantification	20
2.4.4 Starch Extraction and Quantification	21
2.5 statistical analysis	22
3. Results	22

3.1 Photosynthetic activity	22
3.1.1 Light response curves	22
3.1.2 Photosynthetic pigments.....	27
3.1.2.1 Chlorophyll- <i>a</i>	27
3.1.2.2 Chlorophyll- <i>b</i>	28
3.1.2.3 Chlorophyll- <i>a</i> and Chlorophyll- <i>b</i> Ratio.....	29
3.1.2.4 Carotenoids	30
3.1.2.5 Total Chlorophylls and Total Carotenoids Ratio	31
3.2 Biomolecules content.....	31
3.2.1 Glucose	31
3.2.2 Starch.....	32
3.2.3 Protein	32
4. Discussion.....	33
4.1 Photosynthetic Activity	33
4.2 Photosynthetic Pigments	34
4.2.1 Chlorophyll- <i>a</i>	34
4.2.2 Chlorophyll- <i>b</i>	35
4.2.3 Chlorophyll- <i>a</i> / Chlorophyll- <i>b</i> Ratio.....	35
4.2.4 Carotenoids	36
4.2.5 Total Chlorophylls and Total Carotenoids Ratio.....	36

4.3 Biomolecule Content	37
4.3.1 Glucose	37
4.3.2 Starch.....	37
4.3.3 Proteins	38
5. Conclusions	38
6. References	39

1. Introduction

1.1 Marine Heatwaves: their Intensification Linked to Climate Change and Effects on Marine Biodiversity

Marine heatwaves (MHWs) are extreme oceanographic events characterized by prolonged periods of anomalously high sea surface temperatures (SST) over a defined area. These events can last from several days to months and often have serious ecological, biological, and socio-economic impacts. As global ocean temperatures rise due to anthropogenic climate change, the frequency, intensity, and duration of MHWs have increased significantly, making them a key indicator of ocean health and climate change effects (Hobday et al. 2016a).

According to the Intergovernmental Panel on Climate Change (IPCC), MHWs are defined as events where SSTs exceed a high threshold, generally the 90th or 99th percentile, relative to the local climatological average for that time of year. This means MHWs are considered rare occurrences that happen at a specific place and time, usually defined by a relative threshold (SROCC, 2019).

Various metrics are used to measure changes in MHWs, including frequency, duration, intensity, spatial extent, and severity (Cheng et al., 2023). Duration refers to the number of consecutive days in which SST exceeds the defined threshold (the event must last at least five days to be classified as a MHW), intensity is measured by how much the SST surpasses the climatological reference threshold, which is often set at the 90th percentile of historical temperatures. Frequency (in terms of events) refers to how many occurrences take place annually (Hobday et al., 2016b).

Hobday et al. (2018) proposed a four-tiered classification system to describe MHW intensity, based on multiples of the local difference between the climatological mean and the 90th percentile (Figure 1.1). These categories are: Moderate (1–2×, Category I): when SSTs are just above the climatological threshold, with low ecological impact, Strong (2–3×, Category II): when the anomaly is significantly higher than the threshold, Severe (3–4×, Category III):

when the heatwave is intense, with temperature anomalies far exceeding the average, and Extreme ($>4\times$, Category IV): when the MHW is exceptionally intense, with temperatures much higher than the threshold, approaching historical records, and these events can cause catastrophic effects, such as widespread coral bleaching and large-scale marine organism mortality (Soares et al., 2023).

The formation of these heatwaves is due to the combination of various local and distant processes and events operating over a wide range of timeframes and geographical areas, and amplified by human-induced changes to the climate system (Mukherjee et al., 2021, Holbrook et al., 2019)

Looking at the primary drivers, one of the most impactful is the interaction between the ocean and the atmosphere. Events like the El Niño–Southern Oscillation (ENSO, a climate phenomenon characterized by periodic variations in sea surface temperatures and atmospheric pressure patterns in the equatorial Pacific Ocean) play an important role in the formation of MHWs (Liu et al., 2021). During these events, the central and eastern Pacific Ocean experiences significant warming due to changes in wind patterns and weakened upwelling of cold, deep water, leading to elevated sea surface temperatures (SSTs), which can persist for months, creating ideal conditions for marine heatwaves in these regions (*Marine Heatwaves: Climate Change and El Niño Driving Increased Frequency, Intensity and Duration*, 2023).

Changes in ocean circulation can also contribute to MHWs by redistributing heat in the upper layers of the ocean. In fact, Marin et al. (2022) identified air-sea heat fluxes as one of the primary drivers of MHWs, but their influence is expected to decrease for heatwaves that penetrate deeper into the water column. For example, variations in the strength and position of ocean currents, such as the Gulf Stream or the Kuroshio Current, can trap and accumulate heat in certain regions (Du et al., 2022). This heat buildup can lead to significant SST anomalies, particularly when combined with atmospheric conditions preventing the dissipation of this heat (Bischof et al., 2023). Slowdowns in upwelling processes, where cold water from deeper ocean layers fails to reach the surface, can further exacerbate warming in coastal areas, contributing to localized MHWs (Wang et al., 2023).

Atmospheric pressure systems, particularly blocking high-pressure systems, are another major driver of MHWs (Holbrook et al., 2019). These systems can act as "atmospheric lids," trapping warm air over the ocean and preventing heat from being transferred away from the sea surface (Vicinanza, 2023). The persistence of these high-pressure systems can create prolonged periods of calm, clear weather, allowing solar radiation to heat the surface waters without being disrupted by wind or cloud cover (Bashiri et al., 2024).

While natural variability plays a role in the occurrence of MHWs, anthropogenic climate change has significantly intensified their frequency, duration, and severity (Pastor, 2019). The IPCC has confirmed that global warming is raising the baseline ocean temperatures, making MHWs more common and intense. As greenhouse gases continue to accumulate in the atmosphere, the heat they trap is absorbed by the oceans, leading to more frequent and severe heatwaves.

Recent studies indicate that MHWs are now 40% more frequent than they were 100 years ago, with the likelihood of these events continuing to rise as global temperatures increase (Oliver et al., 2018) (Figure 1.2). This long-term warming trend means that even small atmospheric or oceanographic changes can push SSTs past critical thresholds, resulting in a MHW (Frölicher et al., 2018). According to Oliver et al. (2019), without aggressive mitigation efforts to curb greenhouse gas emissions, MHWs could become more frequent and last longer, threatening marine biodiversity and the livelihoods that depend on healthy oceans.

In recent years, the southern coast of Portugal, including areas like the Ria Formosa lagoon, has experienced a growing number of marine heatwave events too, and these warming episodes are increasingly frequent and intense (Schleussner et al., 2020). The rising occurrence of these phenomena in this region poses potential risks to marine ecosystems, with significant effects on both local communities and the habitats they depend on. In this region they can disrupt marine biodiversity, affecting commercially important species, like fish and shellfish, which are central to the region's economy. Additionally, MHWs are believed to have a considerable impact on seaweed and seagrass meadows, which are vital components of coastal ecosystems. Prolonged warming periods can cause stress, alter growth patterns, and even lead to widespread die-offs of key species.

These shifts in algal populations and other primary producers can, in turn, have cascading effects throughout the marine food web, further impacting fisheries and ecosystem services.

As marine heatwaves become more common, understanding their local impacts becomes crucial for developing management strategies to protect the region's biodiversity and the livelihoods of communities reliant on marine resources.

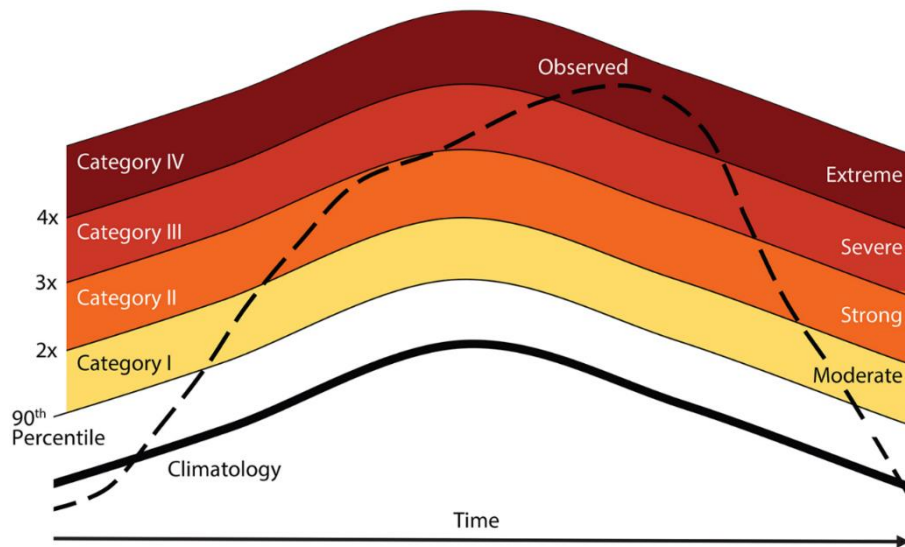


Figure 1.1: Categorization schematic for marine heatwaves (MHWs) defined by Hobday et al. (2018) showing the observed temperature time series (dashed line), the long-term regional climatology (bold line), and the 90th percentile climatology (thin line). Multiples of the 90th percentile difference (2× twice, 3× three times, etc.) from the mean climatology value define each of the categories I–IV, with corresponding descriptors from moderate to extreme. This example peaked as a Category IV (extreme) MHW.

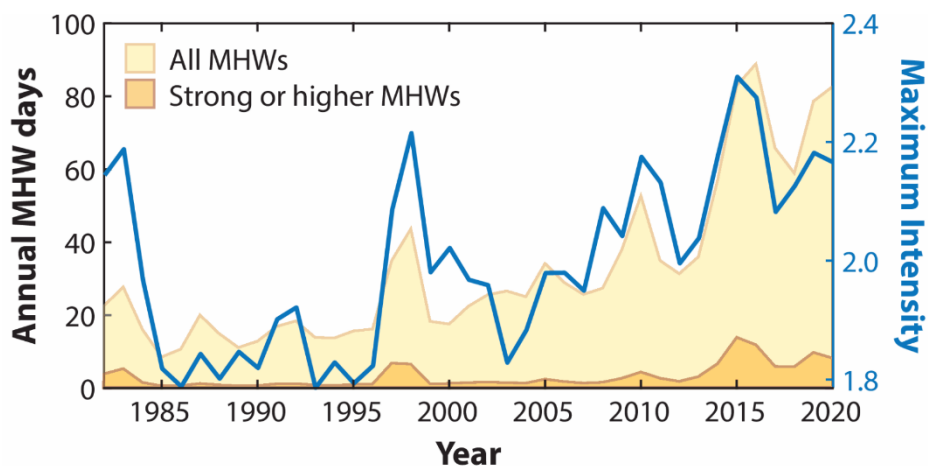


Figure 1.2: Time series of the number of days annually that had MHW conditions of any severity level (yellow) and that had MHW conditions categorized as strong or higher (orange), as defined by Hobday et al. (2018), with the associated maximum intensity superimposed (blue).

1.2 *Ulva* spp. and their Ecological Role

Ulva spp., many of which are known as sea lettuce, are macroalgae in the Ulvophyceae class, the primary multicellular branch of Chlorophyceae (Dawes, 2016). They are frequently found in shallow marine environments and in nutrient-rich, eutrophic waters containing nitrogen and phosphorus (Baweja et al., 2016). Due to their abundance and ease of cultivation, *Ulva* species serve as an ideal biological model and are of great interest in ecological and biotechnological research (Wichard et al., 2015).

Species within the *Ulva* genus play a critical role in coastal ecosystems, providing habitat and food for a wide range of marine organisms, including invertebrates and fish. For example, the blue crab (*Callinectes sapidus*) finds refuge from predators in *Ulva lactuca*, which also serves as a nursery habitat (“Predation Rates on Juvenile Blue Crabs in Estuarine Nursery Habitats: Evidence for the Importance of Macroalgae (*Ulva lactuca*) on JSTOR,” n.d.). Dense algal forests (including those of *Ulva* spp.) serve as nurseries for marine life and help enrich the surrounding waters with oxygen (Cotas et al., 2023).

Additionally, *Ulva* spp.’s nutrient-absorbing capacity makes it valuable for bioremediation, defined by Kensa (2011) as “an ecologically sound and advanced technique that uses natural biological processes to eliminate toxic contaminants.” By absorbing nutrients, *Ulva* spp. reduces nitrogen and phosphorus compounds typically found in polluted waters, thereby improving water quality. For instance, a study by Rahhou et al. (2023) found that *Ulva lactuca* in Nador Lagoon has the potential to bioaccumulate heavy metals and mitigate eutrophication. This effect is especially valuable in lagoon environments and integrated aquaculture systems, where *Ulva* species are used to filter water and reduce excess nutrients. A notable example is the study conducted by Shahar & Guttman (2020) on the species *Ulva fasciata*.

The ecosystem services provided by *Ulva* spp. include carbon sequestration (Park et al., 2024), regulation of biogeochemical cycles (De Clerck et al., 2018), and reduction of ocean acidification (Gao et al., 2019).

However, under certain environmental conditions, *Ulva* spp. can grow excessively, causing harmful algal blooms that may smother other marine life and disrupt ecological balance (Fort et al., 2019). These blooms, commonly known as "green tides," occur mainly in eutrophic waters and can negatively impact local economies, particularly in tourism and fisheries (Smetacek & Zingone, 2013).

Ulva spp. are also the focus of numerous studies due to their biotechnological potential; their ability to accumulate large amounts of biomass makes them promising candidates for biofuel and biomaterial production (Simon et al., 2022; Chemodanov et al., 2017). Moreover, *Ulva* spp. and other macroalgae are playing a growing role in the human food industry, especially in Asia, where they are consumed as nutritious marine vegetables rich in proteins, vitamins, and minerals (Juul et al., 2024; Roleda & Heesch, 2021).

1.3 Influence of MHWs on Algal Communities and the Role of Thermal Priming

Over recent decades, marine heatwaves have significantly impacted marine ecosystems, leading to phenomena, such as the loss of kelp forests (Wernberg et al., 2016), high mortality rates among marine invertebrates (Oliver et al., 2017), and restructuring of marine communities (Bennet et al., 2015).

Many effects of MHWs on algal communities have been thoroughly studied, revealing that intense warming events can impair essential physiological functions, like photosynthesis and respiration, as well as alter community composition and biodiversity (Bernal-Ibáñez et al., 2022; Gouvêa et al., 2017). For instance, in Western Australia, marine heatwaves have disrupted seasonal growth rates and led to a significant rise in mortality among encrusting coralline algae (Short et al., 2015). Between 2014 and 2016, *Nereocystis luetkeana* forests along the California coasts, typically resilient to various stresses, experienced an abrupt and unprecedented decline due to marine heatwaves (McPherson et al., 2021).

Temperature fluctuations directly affect respiration and photosynthesis in algae, as shown in studies on coralline algae, where respiration rates tend to increase within

a certain temperature range but drop sharply with even a slight rise in temperature under MHW-simulated conditions (Adey et al., 1973; Williamson et al., 2017).

Recent studies on macrophyte and algal adaptation to heat events have highlighted the effectiveness of “priming” strategies in enhancing resilience to thermal stress (Jueterbock et al., 2021; Wang et al., 2017). This mechanism enables organisms to develop a “stress memory,” improving their capacity to withstand future thermal stress through cellular and molecular changes, including epigenetic and physiological adaptations (Nguyen et al., 2020).

A study on *Gongolaria barbata*, a brown alga, showed that priming affects variables such as maximum photothermochemical efficiency, photosynthetic pigment content, antioxidant activity, and free radical scavenging capacity. Short-term MHWs initially reduced photothermochemical efficiency, which, however, returned to normal with extended exposure. This recovery was attributed to an increase in photoprotective pigments like carotenoids, which help to dissipate excess thermal energy. Additionally, to face the oxidative stress induced by high temperatures, *G. barbata* showed an increase in producing antioxidant compounds, capable of neutralizing reactive oxygen species (ROS) generated during thermal stress (Fabbrizzi et al., 2023).

Research has also explored thermal priming in marine seagrasses, such as *Posidonia australis* and *Zostera muelleri*. In an experiment involving two heatwaves, pre-heated plants maintained better photosynthetic capacity, leaf growth, and chlorophyll content than unprimed plants. Genetic analyses revealed significant regulation of methylation-related genes, suggesting that epigenetic changes may be crucial in the thermal stress memory of these species (Nguyen et al., 2020).

In another study carried out on kelp *Saccharina latissima*, gametophytes were conditioned at 20°C for periods of 2, 4, and 6 weeks before being returned to 5°C. Results showed that 4 weeks of priming increased sporophyte growth by up to 30% compared to unprimed samples. Furthermore, sporophytes from primed gametophytes exhibited prolonged thermal tolerance and increased resistance to high temperatures, up to 24°C (Gauci et al., 2024).

Priming strategies are increasingly being considered not only for natural ecosystem restoration but also for supporting sustainable algal aquaculture (Ibrahim, 2016; Walls et al., 2018). Developing stress-tolerant macroalgae could aid food production and carbon sequestration, vital in both natural marine environments and algal cultivation systems.

Potential impacts of MHWs on *Ulva* sp. remain largely undocumented, and the specific adaptive or acclimation mechanisms this species, along with other macroalgae, might employ to respond to such events are still poorly understood. Determining the range and extent of population survival and their physiological adaptation capabilities in response to these rapid environmental changes could prove essential.

1.4 Main objectives

The main objectives of this study are:

- To assess the physiological response by *Ulva* sp. to marine heatwaves by analysing levels of various biomolecules and measuring photosynthetic activity.
- To investigate potential adaptive responses in *Ulva* sp. by comparing algal specimens exposed to two consecutive heatwaves (where the first heatwave may act as a priming event) with those exposed to a single heatwave.
- To determine differences in physiological resilience between *Ulva* sp. individuals that have undergone priming through an initial heatwave and those exposed to only one heat event.

2. Materials and methods

2.1 Study site

The Ria Formosa Lagoon is a vast wetland located along the Southern coast of Portugal, in the Algarve region. It stretches for about 84 km² from Faro to Cacela Velha and is separated from the Atlantic Ocean by five main sandy islands (Barreta, Culatra, Armona, Tavira, Cabanas) and two peninsulas (Figure 2.1). These islands act as a natural barrier, protecting the lagoon from waves and ocean currents. The Ria Formosa lagoon has a complex and dynamic morphology, characterized by a series of channels, sandbanks, barrier islands, and intertidal areas (Aníbal et al., 2006).

The structure of the lagoon is dominated by:

- Primary and secondary channels: which allow the inflow and outflow of seawater during tidal cycles.
- Intertidal zones: such as salt marshes and seagrass meadows, which emerge or submerge depending on the tide.
- Mobile sandbanks: which form and shift due to the strength of tidal currents (Achab et al., 2014)

This physical configuration changes over time due to sedimentary processes and coastal erosion, influenced by both natural and human factors. Tides play a fundamental role in shaping the hydrodynamics and morphology of the lagoon. The Ria Formosa lagoon is mesotidal, with moderate tidal ranges. The tides are semi-diurnal, meaning there are two high and two low tides each day. Tidal levels can vary from 1 to 3.5 meters, depending on the lunar phase and weather conditions (Ribeiro et al., 2006).

During high tide, ocean water enters the lagoon through inlets (particularly the natural and artificial openings between the barrier islands), flooding the intertidal zones and channels. During low tide, the water recedes, exposing large areas of sand and mudflats, which are crucial for many marine species and birds that depend on these zones for feeding and breeding. Tidal currents are one of the main factors controlling the circulation of water in the lagoon, ensuring the exchange of water and the distribution of nutrients (Falcao et al., 1990)

The water temperature in the Ria Formosa lagoon can vary significantly both seasonally and daily, influenced by the tide and weather conditions. Temperature variations are due to the shallow depth of the lagoon and its exposure to solar radiation. In summer, water temperatures can reach 28-30°C, especially in the inner areas, which are less directly influenced by ocean currents. Shallow and enclosed waters tend to heat up very quickly. In winter, temperatures can drop to 12-15°C, but the water generally remains warmer than the open ocean due to the heating of the shallow areas (Newton & Mudge, 2003)

This temperature variation can have a significant impact on the lagoon's ecosystems, affecting the metabolic rates of organisms, the life cycles of marine species, and the biodiversity dynamics (Massa et al., 2008).

Moreover, marine heatwaves are becoming more frequent due to climate change and they can cause excessive warming of the lagoon, leading to thermal stress for many species, including seagrass meadows and fish populations. Warmer waters can also reduce the oxygen solubility, leading to hypoxia in some areas of the lagoon (Pimentel & Da Rosa, 2023).

This lagoon is one of the most important natural reserves in Europe, protected by the Parque Natural da Ria Formosa, established in 1987, and is also safeguarded under the Ramsar Convention and the Natura 2000 network (Newton et al., 2022).



Figure 2.1: View of the Ria Formosa lagoon on the South coast of Portugal. *Ulva* sp. sampling sites

2.2 Experimental design

2.2.1 *Ulva* sp. collection

The specimens used for the experiment were adult individuals collected from the Ria Formosa lagoon. They were subsequently cultured and acclimatized in a tank at the hydrobiological station, maintained at a temperature of 18°C.

While we know that these specimens belong to the genus *Ulva*, genetic analyses were not conducted to confirm the specific species. At the beginning of the experiment, the algae were in excellent condition.

2.2.2 Mesocosm experiment setup

The experiment was conducted at the Ramalhete station inside a container room, making it an indoor mesocosm experiment ("common garden" design). Fifteen 35-liter plastic buckets (5 replicates per treatment, n=5) were prepared and filled with water collected from the Ria Formosa through an open system (Figure 2.2).

The Ria Formosa water was stored in a tank outside the container, where it was kept at 15°C using the ECLI20MA IKOMFORTRC900 inverter system, i-Komfort, Kripsol, Toledo, Spain. To reduce microalgal growth, the water was filtered through string-wound and mesh filters that were frequently cleaned and passed through a 50-W UV filter before entering the circuit. The water was aerated and kept in motion with a uniform temperature in the buckets throughout the water column using a bubbling air pipe. After passing through the buckets, the water was filtered and discarded, not reused, and released back into the environment.

To simulate natural light, LED lamps (Ledvance Flood LED 50W/6500K WT, Augsburg, Germany) were used, turning on at 6 AM and off at 9 PM to recreate a 15h:9h photoperiod, ensuring roughly the same light intensity over all the buckets within a range of 400 to 700 nm. The lights were calibrated using a LI-250A Light Meter and a LI-190R sensor (LiCor, USA), with the sensor placed at the surface level of the buckets. The light intensity above each bucket ranged between 130

and $140 \mu\text{mol m}^2 \text{s}^{-1}$ and was then reduced to the $30\text{-}40 \mu\text{mol m}^2 \text{s}^{-1}$ range using three layers of mesh filter.

The air temperature inside the container was kept constant at 20°C using an air conditioner.

The water temperature inside the buckets was controlled by two different systems: the Aquatronica aquarium controller system (ACQKIT115-DL KIT CONTROLLER EVOLUTION DELUXE, Italy) and the Elitech STC-1000Pro temperature controller thermostat by Elitech UK. The Aquatronica system could both maintain the temperature and automatically log it every 15 minutes, managed through the Aquatronica System Controller program, version 9.1.0.0. The Elitech control system could maintain the set temperature but could not record it. To monitor the temperature inside the buckets with this system, HOBO temperature loggers were placed inside, recording the temperature every minute. Both systems were connected to heaters (TMC Therm 200w Digital Aquarium Heater), which were placed inside the buckets along with the temperature sensors. The temperature control systems were tested for a week and calibrated with a digital thermometer (Hanna Instruments HI98509N 1 Checktemp).

The buckets were periodically cleaned to remove any epiphytes and microalgae accumulating on the surface.



Figure 2.2: Pictures of the experimental setup (a) and a view from the top of one aquarium with *Ulva* sp. Inside (b).

2.2.3 Experimental and sampling design

After a selection process to identify individuals in optimal condition, the *Ulva* sp. specimens were placed into the tanks in roughly equal amounts. The three treatments, Single Heatwave (SH), Double Heatwave (DH), and Control (C), were randomly assigned to the 15 tanks. The algae were left at 18°C for 7 days to acclimate to the new environment. During the experiment, the control tanks remained at a constant 18°C, the SH treatment tanks underwent a single heatwave, and the DH treatment tanks experienced two heatwaves. As shown in the diagram, the second heatwave in the DH treatment coincided with the first heatwave SH treatment.

The heatwave simulation was conducted as follows: after the 7-day acclimation period at 18°C, the temperature was increased by 1°C per day until it reached 24°C. Once the peak temperature was achieved, it remained steady for 7 days. After the peak, the temperature was gradually decreased by 1°C per day until it returned to 18°C, where it stayed for 7 days (recovery period). Sampling points, indicated by the red markers, occurred at the start, at the end of the temperature peaks, and at the conclusion of the recovery period (Figure 2.3).

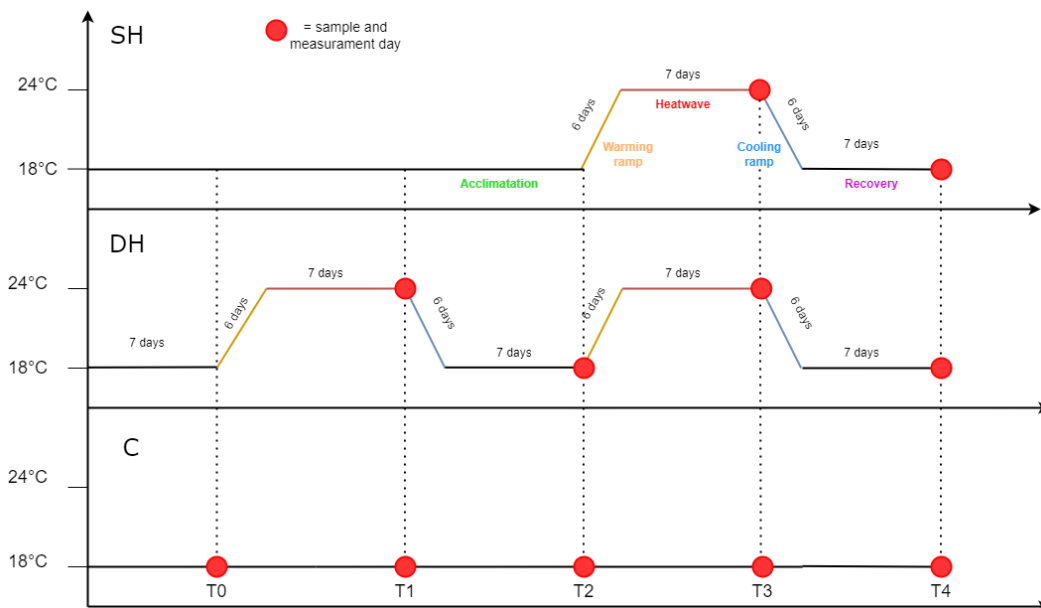


Figure 2.3: Experimental Design Overview: The study included three treatments: Single Heatwave (SH), Double Heatwave (DH), and Control (C). Each heatwave treatment consisted of a warming-up ramp (orange), followed by 7 days of heatwave exposure (red), and concluded with a cooling-down ramp (light blue). The red dots indicate the specific time points when samples were collected (n=5) for each treatment.

2.3 Photosynthetic activity: Photosynthesis-Irradiance (P-I) response curve

To obtain the P-I curves, samples of *Ulva* sp. were collected at time points T1, T2, T3, and T4, corresponding to the end of the HW peaks and after the recovery phase. Samples were carefully taken, cutting as little tissue as possible to minimize stress on the specimen. For each sample, a section of approximately 10 cm² was cut and immediately placed in a polystyrene box to be transported in the dark to the experimental setup.

The setup for the P-I curves consisted of five independent and sealed chambers, each containing a PVC container covered by a petri dish, with an optical O₂ sensor placed on top (Figure 2.4). These containers were equipped with a closed-circuit thermostatic water-bath temperature controller (Julabo HC, Julabo Labortechnik, Seelbach, Germany), capable of maintaining constant water temperature inside. For the control (C) or recovery phase (T2, T4 for DH and T4 for SH), the temperature was set to 18°C. For samples taken at the end of the HW (T1, T3 for DH and T3 for SH), the temperature was set to 24°C.

Light energy was provided by five LED lamps, which could be adjusted in proximity or dimmed using photographic filters. Depending on their position (closer or farther from the algal sample) and the combination of filters, a specific amount of light was emitted, previously measured and calibrated. The containers were filled with water taken from the buckets, which had been filtered through a system using a vacuum gas pump and 0.45 µm cellulose acetate membrane filters (GE Healthcare, Whatman, Germany). Gaseous nitrogen was added to the water to minimize oxygen levels.

Once a chamber was filled, the *Ulva* sp. sample was carefully placed on a support mesh inside, ensuring it was centred and flat. The chamber was then immediately sealed with the petri dish containing the sensor, ensuring no air bubbles formed, as these last ones could increase oxygen levels. A magnetic stirrer ensured water homogenization inside the chambers.

Oxygen content was measured using a portable Fibox 4 trace oxygen meter, equipped with an SP-PSt6 optical sensor and polymer optical fiber (PreSens Precision Sensing GmbH, Germany). At the beginning and end of each P-I curve,

dark respiration was measured: all chambers were covered with a black cloth for 20 minutes. After dark respiration measurements, the five samples (corresponding to the five replicates of each treatment) were incubated at eight increasing levels of Photosynthetically Active Radiation (PAR), ranging from 4 to 1014 $\mu\text{mol photons m}^{-2} \text{s}^{-1}$. The eight PAR levels were selected to ensure accurate representation of the P-I curve shape for each replicate. Each incubation lasted 8 minutes, during which the initial and final oxygen levels were measured.

Throughout the measurements, O_2 saturation levels were periodically monitored, and the incubation duration was adjusted to prevent O_2 supersaturation in the chamber, as this could inhibit photosynthesis and cause fluctuations in pH. Once the oxygen measurements for the curve were completed, each sample was removed from the cuvette and placed in pre-weighed aluminium envelopes. The samples were then allowed to dry in a Heratherm™ General Protocol Incubator, natural convection, 75 L, IGS60 (Thermo Fisher Scientific, Waltham, MA, USA) for three days. After drying, the samples were weighed, and the dry weight was calculated by subtracting the weight of the envelope.

Net photosynthesis (NP) and dark respiration (DR) were calculated using the following formula:

$$NP, DR = \frac{\frac{[\text{O}_2]_f - [\text{O}_2]_i}{T} \times V}{DW}$$

Where:

NP= net photosynthesis

DR= dark respiration

$[\text{O}_2]_f$ = final oxygen concentration

$[\text{O}_2]_i$ = initial oxygen concentration

T = incubation time

V= chamber volume

DW= dry weight

Gross photosynthesis was then calculated by taking dark respiration into account using the following formula:

$$GP = NP + DR$$

To construct the P-I curves, values of gross photosynthesis were used to avoid negative values. Mathematical models were employed, based on the equations:

$$(1) P = P_m [\alpha I / (P_m + \alpha I)], \text{ Henley (1993)}$$

$$(2) P = P_m [\alpha I / (P_m^2 + (\alpha I)^2)^{1/2}], \text{ Smith (1936) and Talling (1957)}$$

$$(3) P = P_m \tanh (\alpha I / P_m), \text{ Jassby e Platt (1976)}$$

$$(4) P = P_m [\alpha I / (P_m^c + (\alpha I)^c)^{1/c}], \text{ Bannister (1979)}$$

$$(5) P = P_s [1 - \exp(-\alpha I/P_s)] \exp(-\beta I/P_s), \text{ Platt et al. (1980)}$$

Where:

P = Photosynthetic rate ($\mu\text{mol O}_2 \text{ gDW}^{-1} \text{ s}^{-1}$)

P_m = Maximum photosynthetic rate ($\mu\text{mol O}_2 \text{ gDW}^{-1} \text{ s}^{-1}$)

I = Irradiance ($\mu\text{mol photons gDW}^{-1} \text{ s}^{-1}$)

α = Ascending slope at limiting irradiances, or photosynthetic quantum efficiency ($\mu\text{mol O}_2 \mu\text{mol photons}^{-1}$)

c = Curvature parameter for the Bannister equation

P_s = maximum theoretical photosynthetic rate in the absence of photoinhibition

β = Irradiance saturation coefficient

The model with the best fit (i.e., with the highest R^2) was used to calculate P_m , α and the half saturation irradiance I_k ($\mu\text{mol photons m}^{-2} \text{s}^{-1}$), according to the following equation:

$$I_k = \frac{P_m}{\alpha}$$

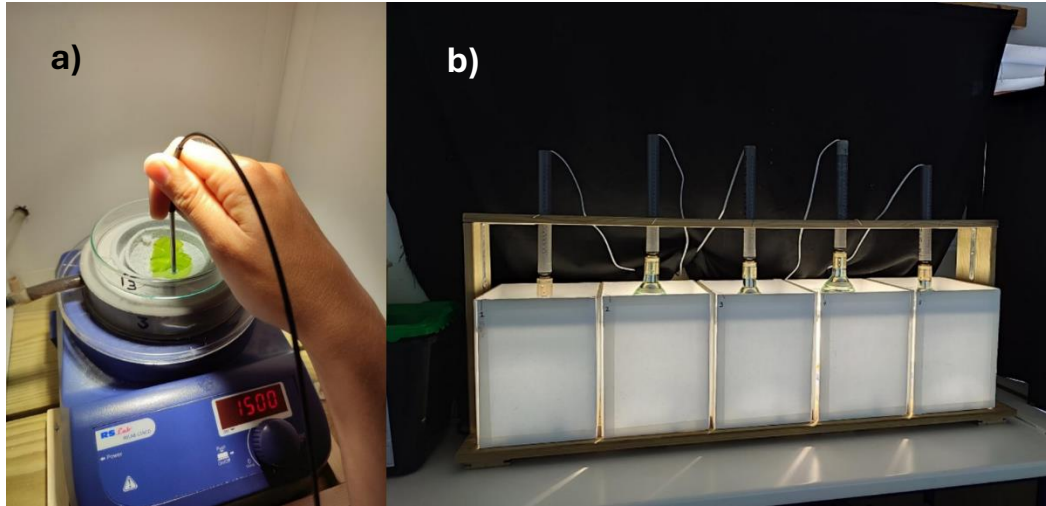


Figure 2.4: Pictures of the setup used to make the P-I curves. a) photo of the PVC chamber containing the algal sample and magnetic stirrer. The measurement of oxygen is shown using the fiber optic cable and oxygen sensor; b) five independent chambers with respective light source.

2.4 Biochemical Composition

Proteins, pigments (chlorophyll *a*, *b*, and carotenoids), sugars, and starch were extracted from *Ulva* sp. samples, collected consistently at the end of the HW peaks and at the end of the recovery phase. Specifically, samples were taken at T0 (5 replicates for the control), T1 (5 for the control and 5 for DH), T2 (5 for the control, 5 for DH), T3 (5 for the control, 5 for DH, and 5 for SH), T4 (5 for the control, 5 for DH, and 5 for SH). On the day of sampling, approximately a handful of different individuals was collected. The algae were then cleaned of any epiphytes, rinsed with distilled water to remove salt, blotted to eliminate excess water, and quickly frozen in liquid nitrogen. Subsequently, the samples were transported and stored in a freezer at -80°C to preserve the biomolecule levels until the day of analysis.

2.4.1 Protein extraction and quantification

The protocol used for protein extraction is based on the Bradford method (1976), in which protein quantification occurs through the Coomassie Brilliant Blue G-250 dye. The blue dye is turned red and primarily protonated (cationic) by the reagent, which is an acidified solution of Coomassie G-250. When the dye interacts with proteins, it binds to the protein's carboxyl groups via Van der Waals forces and to the amino groups via electrostatic interactions. This interaction disrupts the protein's native state, exposing its hydrophobic pockets, which bind non-covalently to the non-polar regions of the dye. As a result, the dye shifts colour from red to blue and its absorbance shifts from 465 nm to 595 nm.

Therefore, the increase in absorbance at 595 nm is proportional to the amount of bound dye, which correlates with the protein concentration in the sample. To quantify protein concentration, a standard curve is generated using known amounts of a standard protein, usually BSA (Bovine Serum Albumin). By comparing the absorbance of the unknown sample to the standard curve, the protein concentration can be determined.

For protein extraction, 0.05 g of sample were weighed and ground in a mortar using liquid nitrogen. Then, 1000 microliters of buffer solution were added, and the mixture was transferred into an Eppendorf tube. The tubes were centrifuged at 4°C for 8 minutes at 15000 g. This procedure was performed for all 55 samples.

To create the calibration curve, 5 dilutions of the standard BSA protein were prepared, with two cuvettes for each dilution, with the following concentrations:

For each sample, two cuvettes were prepared with 780 microliters of Milli-Q water and 20 microliters of sample. To all cuvettes (both those with the samples and those with the solutions for the calibration curve), 200 microliters of Bio-Rad reagent were added, and the contents were mixed with a plastic rod. The cuvettes were then incubated for 10 to 30 minutes (no longer than 30 minutes). It was ensured that the incubation time was as consistent as possible across all samples, with mixing during incubation and just before absorbance reading.

The measurements were conducted using the Compact UV-2700i, a double-beam UV-Vis spectrophotometer, known for its high accuracy and reliability in the ultraviolet and visible light ranges.

2.4.2 Photosynthetic Pigment Extraction and Quantification

Photosynthetic pigments were extracted and quantified from *Ulva* sp. samples using a modified spectrophotometric method according to Lichtenthaler and Buschman (2001). A total of 55 samples were processed for this analysis.

For each sample, approximately 0.100 g of fresh algal tissue was weighed using an analytical balance (with the exact fresh weight recorded) and placed in a small mortar. Liquid nitrogen was then added to the tissue, and the sample was ground thoroughly. A small amount of sodium ascorbate (the tip of a spatula) was added to prevent oxidation, and the grinding process continued with liquid nitrogen.

Following this, 100% methanol was added to the mortar, and the sample was further ground until homogenous. The extract was then transferred to a 5 mL volumetric flask using a glass Pasteur pipette. The mortar was rinsed with additional methanol, and the rinse was also transferred to the volumetric flask. The final volume was adjusted to 5 mL with 100% methanol.

The extracts were centrifuged at 4°C for 10 minutes at 3000 g to remove any solid debris. After centrifugation, the supernatants were collected into 15 mL Falcon tubes and stored in the dark and cold using a foam box lined with aluminum foil and filled with ice. If necessary, the extracts were kept at -20°C until absorbance measurements could be performed.

Before measurements, the extracts were vortexed to ensure homogeneity.

Absorbance readings were taken using a spectrophotometer at wavelengths of 470 nm, 652.4 nm, and 665.2 nm for chlorophyll *a*, chlorophyll *b*, and carotenoids.

The spectrophotometer was turned on 30 minutes before the first reading, and 100% methanol was used as a blank. Absorbance values in the red region of the spectrum were required to be between 0.3 and 0.8. Samples with readings higher than 0.8 were diluted in a 1:2 ratio and remeasured.

Chlorophyll *a* (Chl *a*), chlorophyll *b* (Chl *b*), and total carotenoid (Tcar) concentrations ($\mu\text{g mL}^{-1}$) were calculated using the following equations (Lichtenthaler and Buschman, 2001):

- Chlorophyll *a*: $\text{Chl } a = 16.72 A_{665.2} - 9.16 A_{652.4}$ $\text{Chl } a = 16.72 A_{665.2} - 9.16 A_{652.4}$
- Chlorophyll *b*: $\text{Chl } b = 34.09 A_{652.4} - 4.19 A_{665.2}$ $\text{Chl } b = 34.09 A_{652.4} - 4.19 A_{665.2}$
- Total carotenoids: $\text{Tcar} = (1000 A_{470} - 1.63 \text{Chl } a - 104.96 \text{Chl } b) / 221$ $\text{Tcar} = (1000 A_{470} - 1.63 \text{Chl } a - 104.96 \text{Chl } b) / 221$

Pigment concentrations were expressed on a per dry weight basis.

2.4.3 Non-Structural Carbohydrates Quantification

To quantify the non-structural carbohydrates and starch in *Ulva* sp. samples, a series of extractions and assays were performed using 55 samples. The reagents included 80% ethanol, prepared in bi-distilled or Milli-Q water, 5% phenol solution (5 g in 100 mL, MW = 94.11 g), concentrated sulfuric acid (95.5%), and a glucose stock solution at a concentration of 0.05%, which was prepared by dissolving 50 mg of glucose in 100 mL of bi-distilled or Milli-Q water.

The soluble sugars were extracted following an adapted protocol from Burke et al. (1996). Approximately 0.06 to 0.065 g of fresh or frozen *Ulva* sp. tissue was weighed and ground using liquid nitrogen in a mortar. The tissue was extracted with 4.5 mL of 80% ethanol and transferred to a Falcon tube. The mortar was then rinsed with additional 4.5 mL of 80% ethanol, which was combined with the initial extract. The total volume of the extract was brought to 10 mL with 80% ethanol. The samples were vortexed thoroughly and incubated in a water bath at 80°C for 30 minutes, with intervals of vortexing at 15-minute. After incubation, the samples were centrifuged at 500g for 5 minutes. The supernatant was collected for soluble sugar quantification, while the pellet was retained for starch quantification. The pellet was stored at -20°C after allowing the ethanol to

evaporate at room temperature. Before measuring the soluble sugars, two small spatula scoops of activated charcoal were added to each sample, followed by vortexing and centrifugation at 3000g for 8 minutes. The supernatant was then used for the quantification assay.

The quantification of soluble sugars was based on a colorimetric method adapted from Dubois et al. (1956). A calibration curve was prepared using a glucose stock solution, with concentrations ranging from 5 to 150 $\mu\text{g}/\text{mL}$. For each sample, 1 mL of the supernatant was combined with 1 mL of 5% phenol solution and 5 mL of 95% sulfuric acid. The mixtures were vortexed and allowed to stand for 10 minutes, followed by a second vortexing. The samples were then left to cool for 30 minutes. Absorbance was measured at 490 nm, with 750 nm readings used to control for any turbidity.

The absorbance values at 490 nm, corrected for turbidity, were plotted against the known glucose concentrations to generate a standard curve. The resulting regression equation was used to calculate the total soluble sugar concentration in the *Ulva* sp. samples.

2.4.4 Starch Extraction and Quantification

Starch extraction was performed using the pellets obtained from the previous sugar extraction process. For each sample, a stock enzyme solution was prepared, consisting of α -amylase (30 U/mg) and amyloglucosidase (AGS) (2.8 U/mL). The buffer solution used for the reaction was sodium acetate 0.2 M at pH 4, made by dissolving sodium acetate in Milli-Q water, adjusting the pH with acetic acid, and bringing the final volume to 1 liter.

The pellet was first homogenized in 1 mL of Milli-Q water. The homogenate was then centrifuged at 2000 rpm for 5 minutes, after which the supernatant was discarded. This washing step was repeated three times to ensure the pellet was thoroughly rinsed. After washing, the pellet was resuspended in 1 mL of Milli-Q water and incubated at 100°C for 5 minutes. After incubation, the mixture was vortexed to ensure complete homogenization.

To begin the enzymatic digestion, 100 μL of the resuspended pellet was transferred to a clean Eppendorf tube, and 500 μL of the enzyme suspension (containing α -amylase and AGS in sodium acetate buffer) was added. The samples were then incubated overnight at 37°C to allow the complete starch hydrolysis. After this incubation, the samples were stored at -80°C for some weeks.

The samples then were centrifuged again at 2000 rpm for 5 minutes. To quantify the glucose released from starch hydrolysis, 250 μL of the supernatant was diluted fourfold by adding Milli-Q water to a final volume of 1 mL. The entire volume was used to measure the glucose concentration, following the colorimetric method described previously for the sugar quantification. The glucose concentration was used as a proxy for starch content in the samples, allowing the calculation of starch equivalents based on glucose measurements.

2.5 Statistical analysis

To analyze the differences between the experimental treatments (C, SH, and DH) across the different time phases (T0, T1, T2, T3, T4), a PERMANOVA (Permutational Multivariate Analysis of Variance) was performed for each response variable using the PRIMER software (version 6.1.11). The analysis was conducted with a Euclidean distance metric and 9999 permutations, ensuring a robust statistical estimate.

3. Results

3.1 Photosynthetic activity

3.1.1 Light response curves

Among the five models tested, the Jassby and Platt (1976) model proved to be the most representative, as it achieved one of the highest R^2 values ($R^2 = 0.714$) and effectively described all curves (Table 3.1).

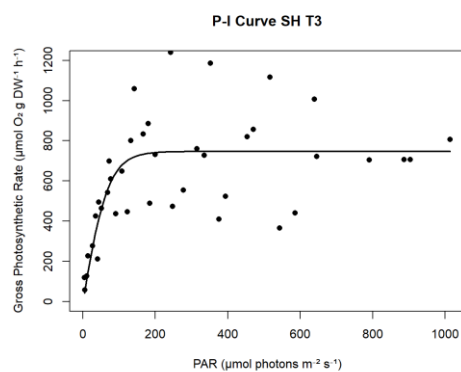
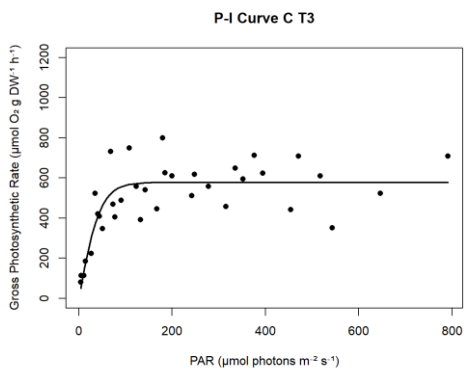
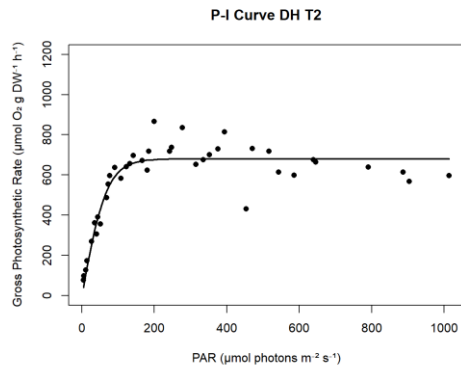
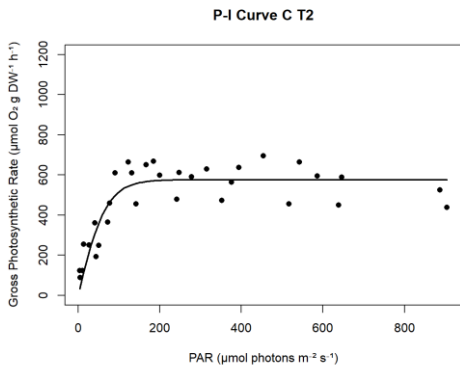
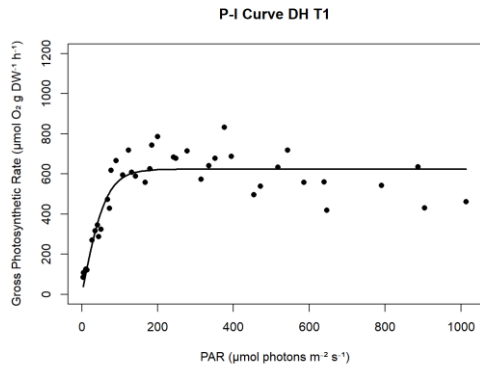
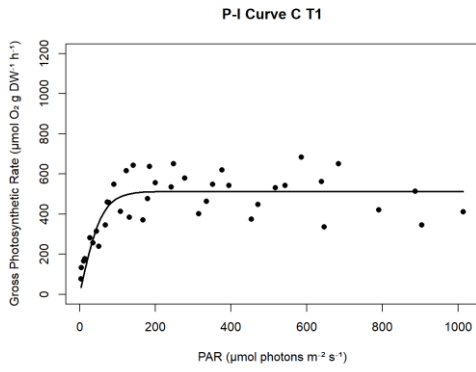
Table 3.1 : *Ulva* sp.'s photosynthetic parameters obtained after fitting the data with the Jassby & Platt (1976) P-I model. Mean photosynthetic quantum efficiency (α ; $\mu\text{mol O}_2 \mu\text{mol photons}^{-1}$), maximal photosynthetic rate (P_m ; $\mu\text{mol O}_2 \text{gDW}^{-1} \text{h}^{-1}$), and half-saturation irradiance (I_k ; $\mu\text{mol photons m}^{-2} \text{s}^{-1}$) are expressed as values \pm SE, for each treatment, of observations (n).

Treatment	Mathematical model				
	Jassby e Platt (1976)	Smith (1936) and Talling (1957)	Henley (1993)	Bannister (1979)	Platt et al. (1980)
T1C	0.63	0.62	0.6	0.63	0.66
T1DH	0.78	0.75	0.68	0.7	0.85
T2C	0.77	0.76	0.72	0.78	0.8
T2DH	0.86	0.85	0.79	0.86	0.9
T3C	0.65	0.65	0.63	0.65	0.65
T3DH	0.7	0.7	0.66	0.7	0.71
T3SH	0.51	0.51	0.49	0.51	0.51
T4C	0.67	0.65	0.59	0.67	0.72
T4DH	0.71	0.7	0.67	0.7	n/a
T4SH	0.86	0.85	0.8	0.86	0.92
Mean R²	0.714	0.704	0.663	0.706	0.746

As shown in the graphs, the P-I curves of *Ulva* sp. described using the Jassby and Platt (1976) equation follow a hyperbolic pattern (Figure 3.1).

At low light intensities, the photosynthetic rate increased linearly with light intensity. This initial trend was characterized by the parameter α , which represents the initial photosynthetic efficiency. As light intensity continues to increase, the curve began to bend and eventually reaches P_{max} , the maximum or saturation point of photosynthesis. The I_k value (half-saturation light intensity) represents the light intensity at which the photosynthetic rate reaches half of P_{max} .

In this model, the curve asymptotically approached P_{max} , indicating there was no photoinhibition (a decrease in the photosynthetic rate) even at high light intensities.



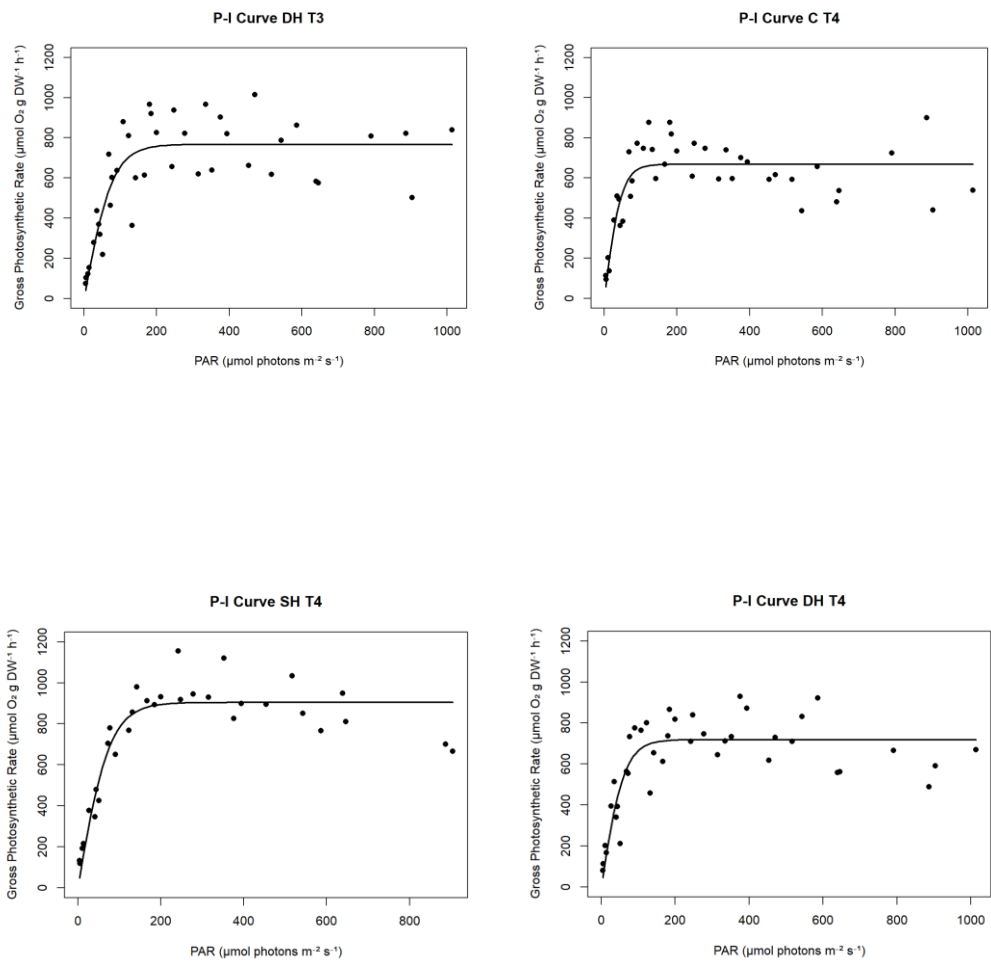


Figure 3.1: P-I curves of *Ulva* sp. from control (C), single heatwave (SH), and double heatwave (DH) treatments at time points T1, T2, T3, and T4. These curves were fitted using the Jassby & Platt (1976) model equation.

Using this model, values for Pmax, α , and Ik were calculated for each treatment, along with their respective standard errors (Table 3.2).

Table 3.2: *Ulva* sp.'s photosynthetic parameters obtained after fitting the data with the Jassby & Platt (1976) P-I model. Mean photosynthetic quantum efficiency (α ; $\mu\text{molO}_2 \mu\text{mol photons}^{-1}$), maximal photosynthetic rate (Pm; $\mu\text{mol O}_2 \text{gDW}^{-1} \text{h}^{-1}$), and half-saturation irradiance (Ik; $\mu\text{mol photons m}^{-2} \text{s}^{-1}$) are expressed as values \pm SE, for each treatment, with corresponding R² and number of observations (n).

Treatment	Pmax	SE	α	SE	Ik	SE	n
CT1	512.33	\pm 18.63	8.72	\pm 1.46	58.77	\pm 10.05	40
CT2	576.22	\pm 20.24	8.33	\pm 1.16	69.18	\pm 9.97	32
CT3	577.78	\pm 23.59	12.60	\pm 2.23	45.87	\pm 8.33	40
CT4	668.00	\pm 22.48	14.31	\pm 2.27	46.67	\pm 7.58	40
DHT1	623.53	\pm 18.84	9.71	\pm 1.18	64.22	\pm 8.08	40
DHT2	680.02	\pm 15.46	10.04	\pm 0.90	67.71	\pm 6.26	40
DHT3	767.17	\pm 30.52	9.78	\pm 1.43	78.42	\pm 11.93	40
DHT4	719.04	\pm 24.33	11.65	\pm 1.62	61.71	\pm 8.85	40
SHT3	746.70	\pm 41.84	10.62	\pm 2.30	70.31	\pm 15.77	40
SHT4	904.16	\pm 25.39	11.84	\pm 1.27	76.35	\pm 8.45	32

Using the five replicates for each treatment, statistical analyses were performed to compare the parameters Pmax, α , and Ik across treatments over different time points. Significant differences in the parameters Pmax and Ik were found between treatments DH and C, as well as between treatments SH and C, within the time points T1, T3, and T4 (Table 3.3 and Figure 3.2). In all cases, both SH and DH parameters were higher than those of the C treatment.

Table 3.3: The table presents treatment pairs that showed a significant difference, specifying the parameters with observed differences and their corresponding p-values.

Comparison	Parameter	p-value
CT2 vs DHT2	Pmax	0.00216
CT3 vs DHT3	Ik	0.0162
CT4 vs SHT4	Ik	0.0229
CT3 vs DHT3	Pmax	0.0409
CT4 vs SHT4	Pmax	0.0084

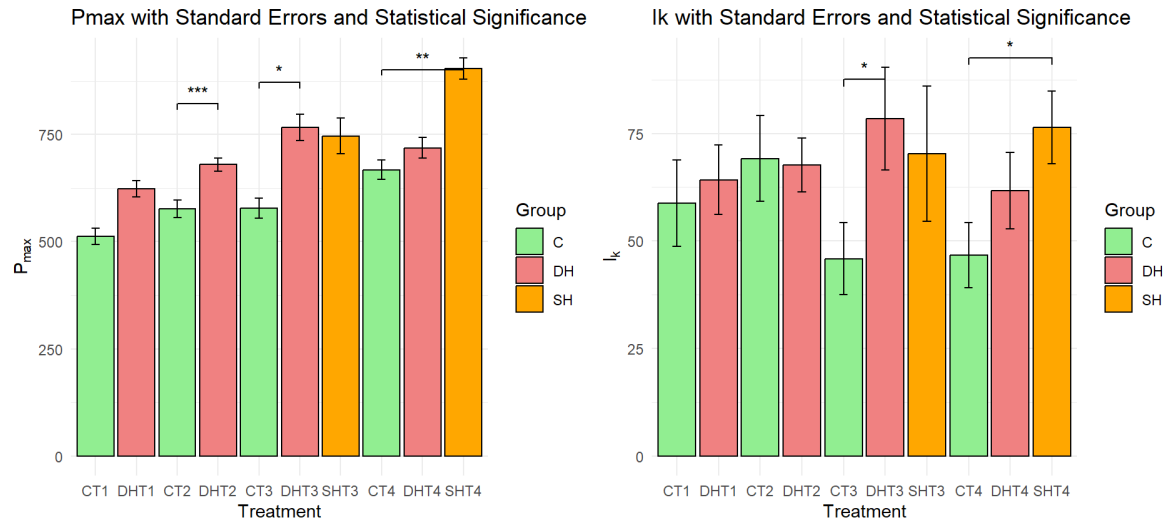


Figure 3.2: The image displays two bar charts illustrating the effects of different treatments on photosynthetic parameters. The chart on the left represents the maximum photosynthetic rate (P_{max} ; $\mu\text{mol O}_2 \text{gDW}^{-1} \text{h}^{-1}$) for each treatment at each time point, with color-coded bars to differentiate treatment groups (C, DH, SH). Associated error bars indicate the standard error (SE P_{max}) for each group. The chart on the right shows the half-saturation irradiance (I_k ; $\mu\text{mol photons m}^{-2} \text{s}^{-1}$) for each treatment, with error bars (SE I_k) representing data variability. Annotations above pairs of bars denote the statistical significance of comparisons between specific groups, marked with a single asterisk (*) for $p < 0.05$, two asterisks (**) for $p < 0.01$, and three asterisks (***) for $p < 0.001$.

3.1.2 Photosynthetic pigments

3.1.2.1 Chlorophyll-*a*

Chlorophyll-*a* levels exhibited similar trends in the three treatments, except at timepoint T3 (coinciding with the second peak), where the DH treatment was significantly higher than both C and SH (p -value= 0.048 and p -value=0.042). At T1, corresponding to the first peak, DH also showed an almost significant deviation from the control (P -value= 0.061). There was a general increase in chlorophyll-*a* levels in the control, due to algal growth, whereas in the DH treatment, chlorophyll-*a* levels were notably higher at the heatwave peaks (Figure 3.4 and Table 3.4)

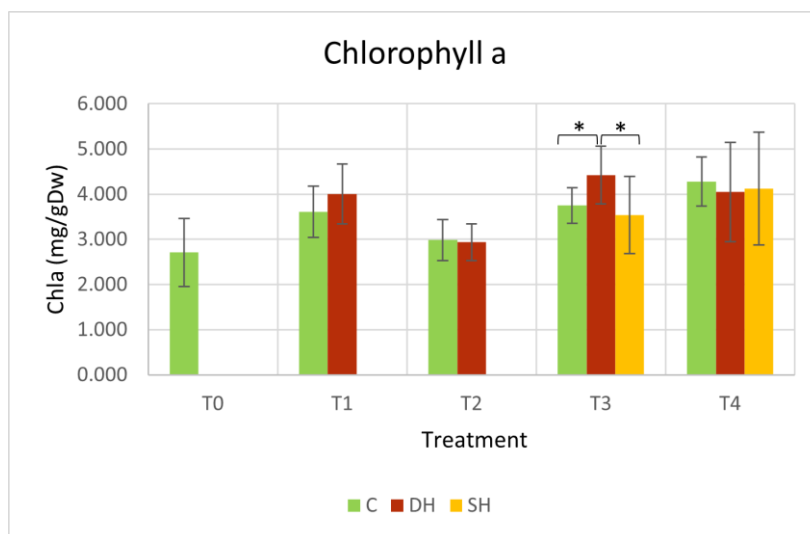


Figure 3.4: Bar chart showing the chlorophyll-a levels in the different treatments at T0, T1, T2, T3, and T4. Error bars represent the associated standard deviation, and asterisks indicate significant differences (single asterisk (*) for $p < 0.05$, two asterisks (**) for $p < 0.01$, and three asterisks (***) for $p < 0.001$).

Table 3.4: Table showing the mean values of Chlorophyll-a for treatments C, DH, and SH at timepoints T0, T1, T2, T3, and T4, along with standard deviations.

Chlorophyll-a						
	C	SD	DH	SD	SH	SD
T0	2.710	0.75273829				
T1	3.611	0.57201118	4.003	0.666365		
T2	2.987	0.4533077	2.939	0.407003		
T3	3.748	0.39005536	4.422	0.642067	3.539	0.85907
T4	4.278	0.54588068	4.047	1.094985	4.122	1.24789

3.1.2.2 Chlorophyll-b

Chlorophyll-b levels closely resemble those of chlorophyll-a, following a similar trend. Here too, there is an almost significant difference at T1 between C and DH (P-value = 0.066), between DH and C at T3 (P-value = 0.083), and between DH and SH at T3 (P-value = 0.081).

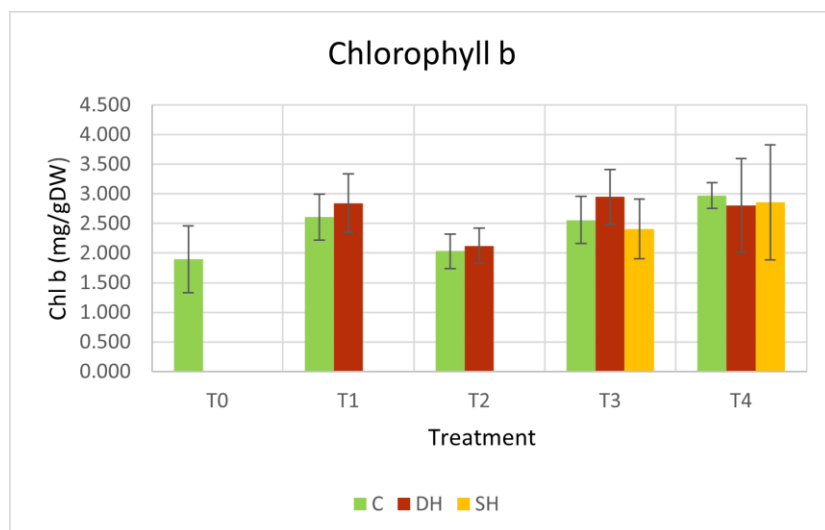


Figure 3.5: Bar chart showing the Chlorophyll-*b* levels in the different treatments at T0, T1, T2, T3, and T4. Error bars represent the associated standard deviation.

Table 3.5: Table showing the mean values of Chlorophyll-*b* for treatments C, DH, and SH at timepoints T0, T1, T2, T3, and T4, along with standard deviations.

Chlorophyll- <i>b</i>						
	C	SD	DH	SD	SH	SD
T0	1.895	0.5659983				
T1	2.607	0.3903551	2.841	0.49424953		
T2	2.032	0.2909133	2.123	0.29552339		
T3	2.558	0.3959094	2.951	0.46158077	2.407	0.500732
T4	2.974	0.2163982	2.804	0.78781108	2.855	0.972486

3.1.2.3 Chlorophyll-*a* and Chlorophyll-*b* Ratio

The trend of the ratio between the two pigments was also observed. A significant difference was found between the C and DH at T2 (P-value= 0.098), corresponding to the first heatwave peak (Figure 3.6).

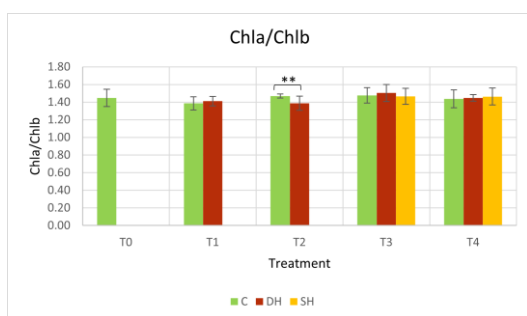


Figure 3.6: Bar chart showing the Chl *a* to Chl *b* ratio levels in the different treatments at T0, T1, T2, T3, and T4. Error bars represent the associated standard deviation, and asterisks indicate significant differences (single asterisk (*) for $p < 0.05$, two asterisks (**) for $p < 0.01$, and three asterisks (***) for $p < 0.001$).

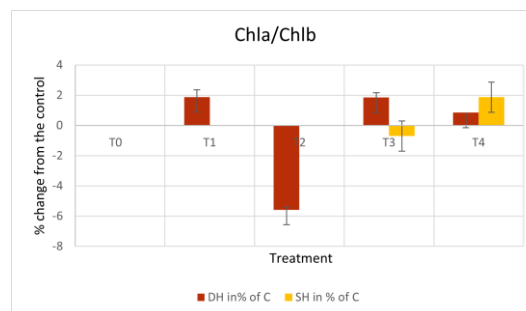


Figure 3.7: Bar chart showing the Chl *a* to Chl *b* ratio expressed as percentage of control in the different treatments at T0, T1, T2, T3, and T4. Error bars represent the associated standard deviation.

The data expressed as a percentage of the control help clarify the difference between the treatments and the control (Figure 3.7).

This result is likely due to the inverse trend between Chl *a* and Chl *b* at T2: in C, Chl *a* is slightly higher than in DH, while for Chl *b*, the opposite is true.

3.1.2.4 Carotenoids

As with chlorophylls, carotenoid levels also showed a significant increase at the heatwave peaks: there is a significant difference between DH and C at T1 (P-value = 0.036), between DH and C at T3 (P-value = 0.048), and between DH and SH at T3 (P-value = 0.038) (Figure 3.8 and Figure 3.9).

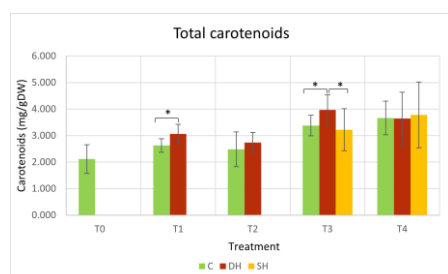


Figure 3.8: Bar chart showing the carotenoids levels of Chl *a* in the different treatments at T0, T1, T2, T3, and T4. Error bars represent the associated standard deviation and asterisks indicate significant differences (single asterisk (*) for $p < 0.05$, two asterisks (**) for $p < 0.01$, and three asterisks (***) for $p < 0.001$).

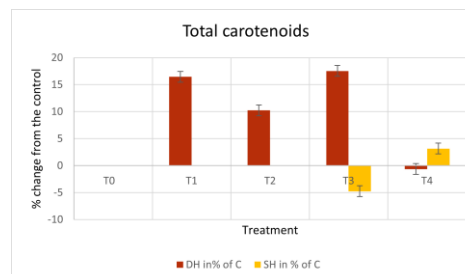


Figure 3.9: Bar chart showing the carotenoids expressed as percentage of control in the different treatments at T0, T1, T2, T3, and T4. Error bars represent the associated standard deviation.

3.1.2.5 Total Chlorophylls and Total Carotenoids Ratio

The ratio between chlorophylls and carotenoids does not vary across treatments, remaining similar throughout. This supports the earlier observation that both carotenoids and chlorophylls increased significantly at the same time points (Figure 3.10)

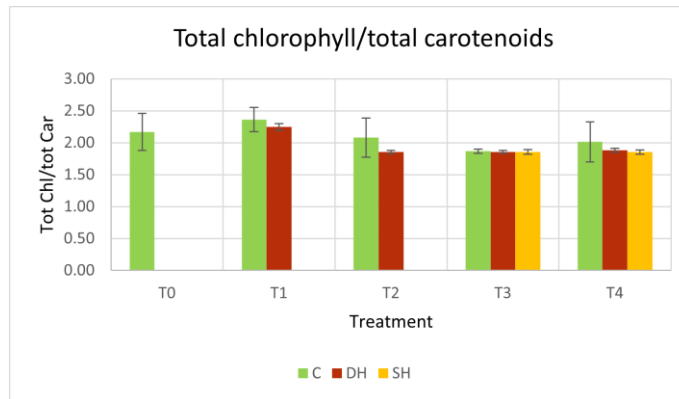


Figure 3.10: Bar chart showing the values of the ratio between total chlorophylls and total carotenoids. Error bars represent the associated standard deviation.

3.2 Biomolecules content

3.2.1 Glucose

The analysis of sugar levels revealed a significant increase in glucose in the DH treatment during the recovery phase after the second peak of the Heatwaves (T4), with a p-value of 0.042. The difference between DH and C at T2 is also nearly significant (Figure 3.11 and Figure 3.12).

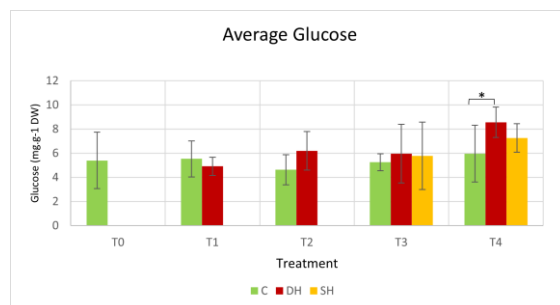


Figure 3.11: Bar chart showing the glucose levels in the different treatments at T0, T1, T2, T3, and T4. Error bars represent the associated standard deviation and asterisks indicate significant differences (single asterisk (*) for $p < 0.05$, two asterisks (**) for $p < 0.01$, and three asterisks (***) for $p < 0.001$).

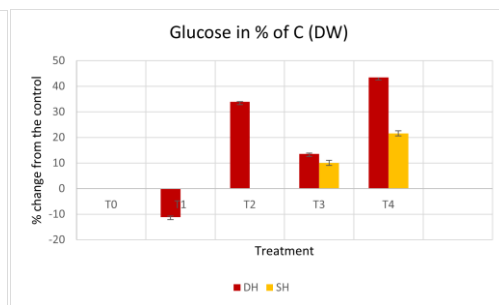


Figure 3.12: Bar chart showing the glucose expressed as percentage of control in the different treatments at T0, T1, T2, T3, and T4. Error bars represent the associated standard deviation.

3.2.2 Starch

For starch, DH showed a significantly lower level than the control one after the first peak (T1), with a p-value of 0.046. No significant differences are observed in the other treatments (Figure 3.13).

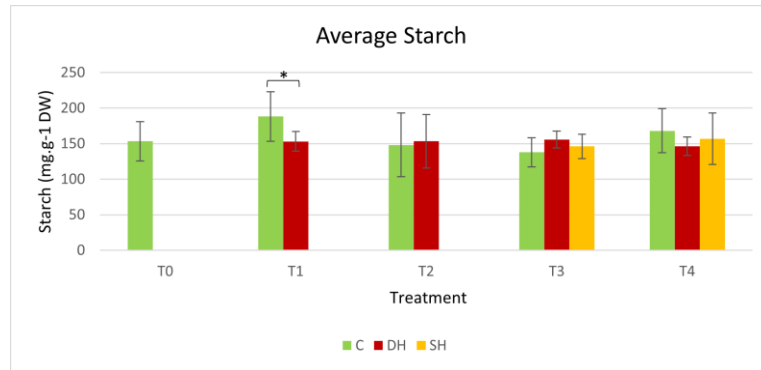


Figure 3.13: Bar chart showing the glucose levels in the different treatments at T0, T1, T2, T3, and T4. Error bars represent the associated standard deviation and asterisks indicate significant differences (single asterisk (*) for $p < 0.05$, two asterisks (**) for $p < 0.01$, and three asterisks (***) for $p < 0.001$).

3.2.3 Protein

For proteins as well, there is a significant difference between DH and C (P-value = 0.029) and between DH and SH (P-value = 0.031) at the second heatwave peak (T3) (Figure 3.1.4), similarly to the pattern observed for chlorophyll-*a* and carotenoids.

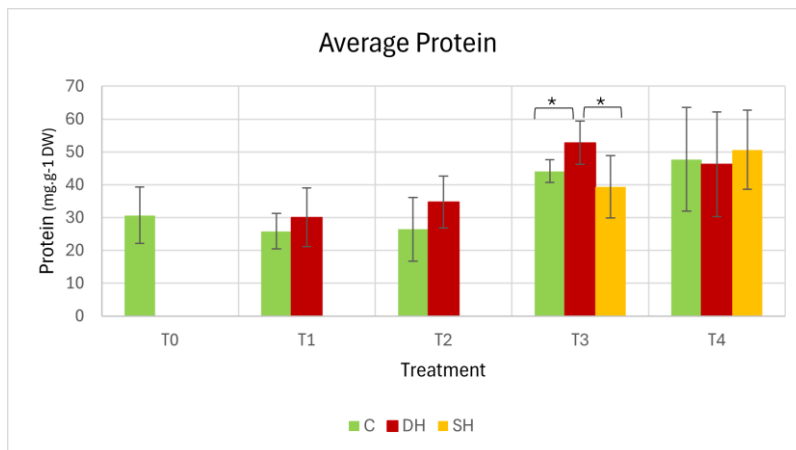


Figure 3.14: Bar chart showing the protein levels in the different treatments at T0, T1, T2, T3, and T4. Error bars represent the associated standard deviation and asterisks indicate significant differences (single asterisk (*) for $p < 0.05$, two asterisks (**) for $p < 0.01$, and three asterisks (***) for $p < 0.001$).

4. Discussion

The analysis of the photosynthetic parameters of *Ulva* sp. and the levels of biomolecules revealed a physiological response to thermal stress induced by heatwaves.

4.1 Photosynthetic Activity

Regarding photosynthetic activity, *Ulva* sp. in both SH (single heatwave) and DH (double heatwave) treatments showed a significant increase in photosynthetic activity (measured by the Pmax parameter) during peak heatwave phases and recovery periods, but this response differed between treatments. Specifically, in the DH treatment, Pmax was higher than the control during the first recovery phase (T2) and at the peak of the second heatwave (T3).

The increase in Pmax at the end of the heatwave may be due to possible hypotheses:

- Adaptation to high temperatures, thanks to the significant plasticity of *Ulva* species and its high thermal tolerance, which represents the result of living in intertidal environments. For instance, studies on the thermal adaptation carried out on *Ulva pertusa* and *U. ohnoi* have shown high photosynthetic plasticity, with excellent parameters of survival at temperatures up to 34°C (Zanolla et al., 2019).
- The temporary ability by this organism to manage thermal load as a short-term adaptive response. The increase in photosynthetic activity has been observed in *U. lactuca* under thermal stress, suggesting it could represent a transitory strategy to maximize photosynthesis (Liu & Zou, 2015), and similarly in *Ulva conglobata* (Zou & Gao, 2014). This increase in photosynthetic activity could be due to an increase in photosynthetic pigments, as already observed by Kakinuma et al. (2005) in *U. pertusa*.

However, this response might not be sustainable in the long term. Indeed, in the DH treatment, *Ulva* sp. during the recovery phase after the second heatwave (T4) did not exhibit a higher Pmax than the control. This decrease could indicate:

- A response of photosynthetic stress, possibly due to damage to photosystem II (PSII) or the photosynthetic apparatus, or an accumulation of reactive oxygen species (ROS) (Eggert, 2012).
- Long-term acclimation due to “priming” from the first heatwave. The decrease in Pmax might reduce the energy demand for photosynthesis, allowing the organism to allocate energy towards repairing cellular damage or synthesizing protective molecules, such as carotenoids (which showed a significant increase after the first heatwave). Sampath-Wiley et al. (2008) documented an increase in carotenoids after a decline in photosynthetic rates. In the SH treatment, a significant increase in Pmax in T4 (similar to the first heatwave peak in the DH treatment) suggests an immediate adaptive response, or a good overall response due to the plasticity of *Ulva* sp.

The increase in Ik during the peak of the second heatwave (T3) indicates that *Ulva* sp. requires higher light intensity to reach half of Pmax, which could suggest that the photosystem becomes less efficient at absorbing light under lower intensities, a signal of potential stress. A similar effect was observed in *Ulva conglobata* representing a result of increased temperature and decreased pH (Li et al., 2020).

4.2 Photosynthetic Pigments

Analysis of photosynthetic pigments revealed significant and nearly significant changes in *Ulva* sp. during heatwave peaks (T1 and T3) and recovery phases (T2 and T4). These changes in pigments reflect physiological responses that may indicate both acclimation mechanisms and signals of photosynthetic stress, particularly after the double heatwave treatment (DH).

4.2.1 Chlorophyll-*a*

The significant increase in Chl-*a* in DH compared to C during heat peaks T3 and the almost significant increase observed in the heat peak T1 suggests that *Ulva* species is attempting to compensate for thermal stress by enhancing its photosynthetic apparatus to optimize light capture. Studies carried out in other seaweeds showing an increase in chlorophyll-*a* under stress conditions can be a

mechanism to boost photosynthetic efficiency, maximizing energy production. A study carried out on sterile mutants of *Ulva pertusa* grown at 30°C showed thallus and cellular changes associated with the thermal stress, in particular, thalli appeared dark green in colour, rich in cytoplasmic content and with markedly thickened cell walls. Moreover, an increase in photosynthetic pigments, thus enhancing photosynthetic activity was registered (Kakinuma et al., 2001). Similar results were observed in *Ulva prolifera* (Bao et al., 2022) and in *U. conglobata* (Zou & Gao, 2014b), where higher growth temperatures (25°C) increased pigment synthesis. However, this adaptive response might be transitory and unsustainable in the long term, especially if thermal damage persists, eventually leading to a decrease in chlorophyll to reduce the photosynthetic load. In the SH treatment, although not statistically significant, an increase in Chl-a was observed at T4 during the resting phase following the initial peak. This may also represent an adaptive response to the heatwave, with a more subdued effect likely due to insufficient time for the treatment to fully respond to the heat stress.

4.2.2 Chlorophyll-b

Chl-*b*, present in smaller quantities than Chl-*a*, plays a secondary role in light absorption and protecting the photosynthetic apparatus. The nearly significant differences between DH, control (C), and SH treatments during thermal peaks (T1 and T3) suggest a modulation in pigment composition to optimize light absorption and reduce oxidative stress. An increase in Chl-*b* might indicate that *Ulva* sp. is enhancing pigment diversity to absorb a broader range of wavelengths in response to excessive light associated with thermal stress. Yang et al. (2019) showed an increase in both Chl-*a* and Chl-*b* (although the latter to a lesser extent) in *U. prolifera* after four days at high temperatures. After some time, however, a reduction in these pigments was observed due to accumulated stress.

4.2.3 Chlorophyll-a / Chlorophyll-b Ratio

The high ratio of Chl-*a* to Chl-*b* in T2 for the control treatment compared to DH suggests that *Ulva* sp. under non-stressed conditions (C) maintains a photosynthetic

apparatus with a high proportion of Chl-*a* to maximize photosynthetic efficiency under moderate light conditions. Typically, this ratio tends to increase under higher temperature and stress and remain lower under normal conditions. As observed in this study and in another research carried out on the species *U. prolifera* by Zheng et al. (2019), where Chl-*a* levels tend to increase more than Chl-*b* under stress conditions, the modulation of this ratio in DH could represent a strategy to balance light absorption and excess energy dissipation under stress conditions.

4.2.4 Carotenoids

Carotenoids are known for their antioxidant properties and play an important key role in protecting the photosynthetic apparatus under high light and temperature stress conditions (Stahl & Sies, 2003). The increase in carotenoids in DH during the first thermal peak (T1) indicates *Ulva* sp. is activating its antioxidant protection mechanisms to prevent damage caused by excess ROS, which are often produced in response to thermal stress. For instance, in the study performed on *Ulva rigida* by Cruces et al. (2019), an increase in carotenoids levels was one of the acclimation mechanisms used in response to rapid diurnal changes of light and temperature. The further increase in carotenoids during T3 in DH compared to C and SH suggests that the cumulative effect of two heatwaves further stimulated the production of these protective pigments. This is consistent with observations obtained in other marine algae, where carotenoids increased significantly under chronic stress to protect PSII. A study on *U. prolifera* exposed the algae to three temperatures (12°C, 20°C, and 28°C) and transcriptomic and biosynthetic analyses showed that production and levels of carotenoids responded sensitively to temperature, with an increase in carotenoid concentrations when the algae were exposed to heat stress (He et al., 2018b).

4.2.5 Total Chlorophylls and Total Carotenoids Ratio

The ratio of total chlorophyll to total carotenoids did not show significant differences between any of the treatments. This suggests that chlorophylls and

carotenoids follow a similar trend at each time point, consistent with the previous discussion.

4.3 Biomolecule Content

4.3.1 Glucose

The increase in the glucose level in the DH treatment during the recovery phase (T4) may reflect an energy storage response to support recovery after repeated thermal stress (Diamant et al., 2001). This phenomenon is consistent with observations detected in some algal species, where heat events can temporarily increase the carbohydrate reserves to better withstand adverse conditions. For example, in an investigation performed by He, et al. (2018a), an increase in the accumulation of eight different sugar types was observed in *U. prolifera* under high thermal stress. Among them, glucose accumulated 1.8 times more. These results suggest that high thermal stress alters enzymatic activities related to carbon and starch metabolism and sucrose synthesis by reducing the expression of certain genes associated with carbohydrate metabolism (Yong-Ling et al., 2010).

4.3.2 Starch

The significant reduction in starch in the DH treatment compared to the control during T1 might indicate the mobilization of energy reserves in response to the acute stress condition caused by the first heatwave. Some algae reduce starch levels under stress to support the production of defence compounds or increased cellular respiration. This mechanism leads to an increase in sugars, as observed earlier in this study. Similarly, He, et al. (2018a) suggest that “the Calvin cycle, glycolysis, and adjacent pathways are the primary metabolic processes for heat attenuation, with increased primary productivity in response to HTS (high temperature stress).”

4.3.3 Proteins

The significant increase in protein levels observed in T3 for the DH treatment, compared to C and SH, can be interpreted as an adaptive response of the alga to thermal stress. During the second heat peak, the synthesis of structural and stress-related proteins plays a crucial role in maintaining the integrity of the photosystem and repairing damage caused by excessive heat. A similar mechanism was identified in a study by Kakinuma et al. (2001), where algae exposed to high temperatures exhibited a 1.9 to 10.5-fold increase in protein levels in response to thermal stress (30°C). In a study on *Ulva* sp. and *Porphyra columbina*, it was similarly demonstrated that stress proteins, also known as heat shock proteins (HSPs), play a key role in the defence mechanism, particularly when organisms are subjected to stress from temperature fluctuations and solar radiation (Cruces et al., 2012).

5. Conclusions

In conclusion, *Ulva* sp. demonstrated a well-adapted physiological response to thermal stress induced by heatwaves, utilizing various adaptive mechanisms. The increase in chlorophylls, carotenoids, proteins, and glucose levels observed during the second heatwave suggests that the organism may have developed an adaptive strategy, likely as a result of previous heat exposure. Changes in photosynthetic pigments and photosynthetic activity reflect an attempt to optimize energy production, while the increase in proteins and glucose indicates a metabolic response aimed at cellular protection and recovery.

It would have been interesting to also analyse gene expression related to heat shock proteins (HSPs), reactive oxygen species (ROS) levels, and other stress-response molecules such as lipids, phytochelatins, and antioxidants. These studies could help to deepen our understanding of the cellular mechanisms of adaptation and defence. In the future, conducting experiments with higher temperatures or examining the long-term effects of single or multiple heatwaves would provide valuable insights into the resilience of *Ulva* sp. to prolonged thermal stress.

6. References

- Aníbal, J., Rocha, C., & Sprung, M. (2006). Mudflat surface morphology as a structuring agent of algae and associated macroepifauna communities: A case study in the Ria Formosa. *Journal of Sea Research*, 57(1), 36–46.
<https://doi.org/10.1016/j.seares.2006.07.002>
- Bao, M., Park, J., Xing, Q., He, P., Zhang, J., Yarish, C., Yoo, H. I., & Kim, J. K. (2022). Comparative Analysis of Physiological Responses in Two *Ulva prolifera* Strains Revealed the Effect of Eutrophication on High Temperature and Copper Stress Tolerance. *Frontiers in Marine Science*, 9.
<https://doi.org/10.3389/fmars.2022.863918>
- Bashiri, B., Barzandeh, A., Männik, A., & Raudsepp, U. (2024). Variability of marine heatwaves' characteristics and assessment of their potential drivers in the Baltic Sea over the last 42 years. *Scientific Reports*, 14(1).
<https://doi.org/10.1038/s41598-024-74173-2>
- Baweja, P., Kumar, S., Sahoo, D., & Levine, I. (2016). Biology of Seaweeds. In Elsevier eBooks (pp. 41–106). <https://doi.org/10.1016/b978-0-12-802772-1.00003-8>
- Bennett, S., Wernberg, T., Harvey, E. S., Santana-Garcon, J., & Saunders, B. J. (2015). Tropical herbivores provide resilience to a climate-mediated phase shift on temperate reefs. *Ecology Letters*, 18(7), 714–723.
<https://doi.org/10.1111/ele.12450>
- Bernal-Ibáñez, A., Gestoso, I., Ramalhosa, P., Campanati, C., & Cacabelos, E. (2022). Interaction of marine heatwaves and grazing on two canopy-forming algae. *Journal of Experimental Marine Biology and Ecology*, 556, 151795.
<https://doi.org/10.1016/j.jembe.2022.151795>
- Bischof, S., Kedzierski, R. P., Hänsch, M., Wahl, S., & Matthes, K. (2023). The role of the North Atlantic for heat wave characteristics in Europe, an ECHAM6 study. *Geophysical Research Letters*, 50(23). <https://doi.org/10.1029/2023gl105280>
- Chemodanov, A., Jinjikhshvily, G., Habiby, O., Liberzon, A., Israel, A., Yakhini, Z., & Golberg, A. (2017). Net primary productivity, biofuel production and CO₂ emissions reduction potential of *Ulva* sp. (Chlorophyta) biomass in a coastal area of the Eastern Mediterranean. *Energy Conversion and Management*, 148, 1497–1507. <https://doi.org/10.1016/j.enconman.2017.06.066>
- Cheng, Y., Zhang, M., Song, Z., Wang, G., Zhao, C., Shu, Q., Zhang, Y., & Qiao, F. (2023). A quantitative analysis of marine heatwaves in response to rising sea surface temperature. *The Science of the Total Environment*, 881, 163396.
<https://doi.org/10.1016/j.scitotenv.2023.163396>

- Cotas, J., Gomes, L., Pacheco, D., & Pereira, L. (2023). Ecosystem services provided by Seaweeds. *Hydrobiology*, 2(1), 75–96. <https://doi.org/10.3390/hydrobiology2010006>
- Cruces, E., Huovinen, P., & Gomez, I. (2012). Stress proteins and auxiliary anti stress compounds in intertidal macroalgae. *Latin American Journal of Aquatic Research*, 40(4), 822–834. <https://doi.org/10.3856/vol40-issue4-fulltext-1>
- Cruces, E., Rautenberger, R., Cubillos, V.M., Ramírez-Kushel, E., Rojas-Lillo, Y., Lara, C., Montory, J. A., & Gómez, I. (2019). Interaction of Photoprotective and Acclimation Mechanisms in *Ulva rigida* (Chlorophyta) in Response to Diurnal Changes in Solar Radiation in Southern Chile. *Journal of Phycology*, 55(5), 1011–1027. <https://doi.org/10.1111/jpy.12894>
- Dawes, C. (2016). Macroalgae systematics. In *Elsevier eBooks* (pp. 107–148). <https://doi.org/10.1016/b978-0-12-802772-1.00004-x>
- De Clerck, O., Kao, S., Bogaert, K. A., Blomme, J., Foflonker, F., Kwantes, M., Vancaester, E., Vanderstraeten, L., Aydogdu, E., Boesger, J., Califano, G., Charrier, B., Clewes, R., Del Cortona, A., D'Hondt, S., Fernandez-Pozo, N., Gachon, C. M., Hanikenne, M., Lattermann, L., . . . Bothwell, J. H. (2018). Insights into the Evolution of Multicellularity from the Sea Lettuce Genome. *Current Biology*, 28(18), 2921- 2933.e5. <https://doi.org/10.1016/j.cub.2018.08.015>
- Diamant, S., Eliahu, N., Rosenthal, D., & Goloubinoff, P. (2001). Chemical Chaperones Regulate Molecular Chaperones in Vitro and in Cells under Combined Salt and Heat Stresses. *Journal of Biological Chemistry*, 276(43), 39586–39591. <https://doi.org/10.1074/jbc.m103081200>
- Du, Y., Feng, M., Xu, Z., Yin, B., & Hobday, A. J. (2022). Summer marine heatwaves in the Kuroshio-Oyashio extension region. *Remote Sensing*, 14(13), 2980. <https://doi.org/10.3390/rs14132980>
- Eggert, A. (2012). Seaweed responses to temperature. In *Ecological studies* (pp. 47–66). https://doi.org/10.1007/978-3-642-28451-9_3
- Fabbrizzi, E., Munari, M., Frascetti, S., Arena, C., Chiarore, A., Cannavacciuolo, A., Colletti, A., Costanzo, G., Soler-Fajardo, A., Nannini, M., Savinelli, B., Silvestrini, C., Vitale, E., & Tamburello, L. (2023). Canopy-forming macroalgae can adapt to marine heatwaves. *Environmental Research*, 238, 117218. <https://doi.org/10.1016/j.envres.2023.117218>
- Falcao, M., & Vale, C. (1990). Study of the Ria Formosa ecosystem: benthic nutrient remineralization and tidal variability of nutrients in the water. *Hydrobiologia*, 207(1), 137–146. <https://doi.org/10.1007/bf00041450>
- Fort, A., Mannion, C., Fariñas-Franco, J. M., & Sulpice, R. (2019). Green tides select for fast expanding *Ulva* strains. *The Science of the Total Environment*, 698, 134337. <https://doi.org/10.1016/j.scitotenv.2019.134337>

- Frölicher, T. L., Fischer, E. M., & Gruber, N. (2018). Marine heatwaves under global warming. *Nature*, *560*(7718), 360–364. <https://doi.org/10.1038/s41586-018-0383-9>
- Gao, K., Beardall, J., Häder, D., Hall-Spencer, J. M., Gao, G., & Hutchins, D. A. (2019). Effects of ocean acidification on marine photosynthetic organisms under the concurrent influences of warming, UV radiation, and deoxygenation. *Frontiers in Marine Science*, *6*. <https://doi.org/10.3389/fmars.2019.00322>
- Gauci, C., Jueterbock, A., Khatei, A., Hoarau, G., & Bartsch, I. (2024). Thermal priming of *Saccharina latissima*, a promising strategy to improve seaweed production and restoration in future climates. *Marine Ecology Progress Series*. <https://doi.org/10.3354/meps14683>
- Gouvêa, L. P., Schubert, N., Martins, C. D. L., Sissini, M., Ramlov, F., De Oliveira Rodrigues, E. R., Bastos, E. O., Freire, V. C., Maraschin, M., Simonassi, J. C., Varela, D. A., Franco, D., Cassano, V., Fonseca, A. L., J. B. B., & Horta, P. A. (2017). Interactive effects of marine heatwaves and eutrophication on the ecophysiology of a widespread and ecologically important macroalga. *Limnology and Oceanography*, *62*(5), 2056–2075. <https://doi.org/10.1002/lno.10551>
- He, Y., Hu, C., Wang, Y., Cui, D., Sun, X., Li, Y., & Xu, N. (2018). The metabolic survival strategy of marine macroalga *Ulva prolifera* under temperature stress. *Journal of Applied Phycology*, *30*(6), 3611–3621. <https://doi.org/10.1007/s10811-018-1493-3>
- He, Y., Ma, Y., Du, Y., & Shen, S. (2018). Differential gene expression for carotenoid biosynthesis in a green alga *Ulva prolifera* based on transcriptome analysis. *BMC Genomics*, *19*(1). <https://doi.org/10.1186/s12864-018-5337-y>
- Hobday, A. J., Alexander, L. V., Perkins, S. E., Smale, D. A., Straub, S. C., Oliver, E. C., Benthuyesen, J. A., Burrows, M. T., Donat, M. G., Feng, M., Holbrook, N. J., Moore, P. J., Scannell, H. A., Gupta, A. S., & Wernberg, T. (2016a). A hierarchical approach to defining marine heatwaves. *Progress in Oceanography*, *141*, 227–238. <https://doi.org/10.1016/j.pocean.2015.12.014>
- Hobday, A. J., Alexander, L. V., Perkins, S. E., Smale, D. A., Straub, S. C., Oliver, E. C., Benthuyesen, J. A., Burrows, M. T., Donat, M. G., Feng, M., Holbrook, N. J., Moore, P. J., Scannell, H. A., Gupta, A. S., & Wernberg, T. (2016b). A hierarchical approach to defining marine heatwaves. *Progress in Oceanography*, *141*, 227–238. <https://doi.org/10.1016/j.pocean.2015.12.014>
- Hobday, A., Oliver, E., Gupta, A. S., Benthuyesen, J., Burrows, M., Donat, M., Holbrook, N., Moore, P., Thomsen, M., Wernberg, T., & Smale, D. (2018). Categorizing and naming marine heatwaves. *Oceanography*, *31*(2). <https://doi.org/10.5670/oceanog.2018.205>
- Holbrook, N. J., Scannell, H. A., Gupta, A. S., Benthuyesen, J. A., Feng, M.,

- Oliver, E. C. J., Alexander, L. V., Burrows, M. T., Donat, M. G., Hobday, A. J., Moore, P. J., Perkins- Kirkpatrick, S. E., Smale, D. A., Straub, S. C., & Wernberg, T. (2019). A global assessment of marine heatwaves and their drivers. *Nature Communications*, *10*(1). <https://doi.org/10.1038/s41467-019-10206-z>
- Ibrahim, E. A. (2016). Seed priming to alleviate salinity stress in germinating seeds. *Journal of Plant Physiology*, *192*, 38–46. <https://doi.org/10.1016/j.jplph.2015.12.011>
- Jueterbock, A., Minne, A. J. P., Cock, J. M., Coleman, M. A., Wernberg, T., Scheschonk, L., Rautenberger, R., Zhang, J., & Hu, Z. (2021). Priming of marine macrophytes for enhanced restoration success and food security in future oceans. *Frontiers in Marine Science*, *8*. <https://doi.org/10.3389/fmars.2021.658485>
- Juul, L., Nissen, S. H., Bruhn, A., Alexi, N., Jensen, S. K., Hammershøj, M., & Dalsgaard, T. K. (2024). *Ulva* species: A critical review on the green seaweed as a source of food protein. *Trends in Food Science & Technology*, *149*, 104534. <https://doi.org/10.1016/j.tifs.2024.104534>
- Kakinuma, M., Coury, D. A., Kuno, Y., Itoh, S., Kozawa, Y., Inagaki, E., Yoshiura, Y., & Amano, H. (2005). Physiological and biochemical responses to thermal and salinity stresses in a sterile mutant of *Ulva pertusa* (Ulvales, Chlorophyta). *Marine Biology*, *149*(1), 97–106. <https://doi.org/10.1007/s00227-005-0215-y>
- Kakinuma, M., Shibahara, N., Ikeda, H., Maegawa, M., & Amano, H. (2001). Thermal stress responses of a sterile mutant of *Ulva pertusa* (Chlorophyta). *Fisheries Science*, *67*(2), 287–294. <https://doi.org/10.1046/j.1444-2906.2001.00229.x>
- Kensa, V. M. (2011). BIOREMEDIATION - AN OVERVIEW. *I Control Pollution*, *27*(2), 161–168. <https://www.icontrolpollution.com/articles/bioremediation-an-overview-161-168.pdf>
- Li, G., Qin, Z., Zhang, J., Lin, Q., Ni, G., Tan, Y., & Zou, D. (2020). Algal density mediates the photosynthetic responses of a marine macroalga *Ulva conglobata* (Chlorophyta) to temperature and pH changes. *Algal Research*, *46*, 101797. <https://doi.org/10.1016/j.algal.2020.101797>
- Liu, C., & Zou, D. (2015). Responses of elevated CO₂ on photosynthesis and nitrogen metabolism in *Ulva lactuca* (Chlorophyta) at different temperature levels. *Marine Biology Research*, *11*(10), 1043–1052. <https://doi.org/10.1080/17451000.2015.1062520>
- Liu, K., Xu, K., Zhu, C., & Liu, B. (2021). Diversity of marine heatwaves in the South China Sea regulated by ENSO Phase. *Journal of Climate*, *35*(2), 877–893. <https://doi.org/10.1175/jcli-d-21-0309.1>
- Marin, M., Feng, M., Bindoff, N. L., & Phillips, H. E. (2022). Local drivers of

extreme upper ocean marine heatwaves assessed using a global ocean circulation model. *Frontiers in Climate*, 4. <https://doi.org/10.3389/fclim.2022.788390>

Massa, S. I., Arnaud-Haond, S., Pearson, G. A., & Serrão, E. A. (2008). Temperature tolerance and survival of intertidal populations of the seagrass *Zostera noltii* (Hornemann) in Southern Europe (Ria Formosa, Portugal). *Hydrobiologia*, 619(1), 195–201. <https://doi.org/10.1007/s10750-008-9609-4>

McPherson, M. L., Finger, D. J. I., Houskeeper, H. F., Bell, T. W., Carr, M. H., Rogers-Bennett, L., & Kudela, R. M. (2021). Large-scale shift in the structure of a kelp forest ecosystem co-occurs with an epizootic and marine heatwave. *Communications Biology*, 4(1). <https://doi.org/10.1038/s42003-021-01827-6>

Mukherjee, S., Mishra, A. K., Ashfaq, M., & Kao, S. (2021). Relative effect of anthropogenic warming and natural climate variability to changes in Compound drought and heatwaves. *Journal of Hydrology*, 605, 127396. <https://doi.org/10.1016/j.jhydrol.2021.127396>

Newton, A., Cañedo-Argüelles, M., March, D., Goela, P., Cristina, S., Zacarias, M., & Icely, J. (2022). Assessing the effectiveness of management measures in the Ria Formosa coastal lagoon, Portugal. *Frontiers in Ecology and Evolution*, 10. <https://doi.org/10.3389/fevo.2022.508218>

Newton, A., & Mudge, S. M. (2003). Temperature and salinity regimes in a shallow, mesotidal lagoon, the Ria Formosa, Portugal. *Estuarine Coastal and Shelf Science*, 57(1–2), 73–85. [https://doi.org/10.1016/s0272-7714\(02\)00332-3](https://doi.org/10.1016/s0272-7714(02)00332-3)

Nguyen, H. M., Kim, M., Ralph, P. J., Marín-Guirao, L., Pernice, M., & Procaccini, G. (2020). Stress Memory in seagrasses: First insight into the effects of thermal priming and the role of epigenetic modifications. *Frontiers in Plant Science*, 11. <https://doi.org/10.3389/fpls.2020.00494>

Nielsen, M. M., Bruhn, A., Rasmussen, M. B., Olesen, B., Larsen, M. M., & Møller, H.B. (2011). Cultivation of *Ulva lactuca* with manure for simultaneous bioremediation and biomass production. *Journal of Applied Phycology*, 24(3), 449–458. <https://doi.org/10.1007/s10811-011-9767-z>

Oliver, E. C. J., Benthuyesen, J. A., Bindoff, N. L., Hobday, A. J., Holbrook, N. J., Mundy, C. N., & Perkins-Kirkpatrick, S. E. (2017). The unprecedented 2015/16 Tasman Sea marine heatwave. *Nature Communications*, 8(1). <https://doi.org/10.1038/ncomms16101>

Oliver, E. C. J., Donat, M. G., Burrows, M. T., Moore, P. J., Smale, D. A., Alexander, L.V., Benthuyesen, J. A., Feng, M., Gupta, A. S., Hobday, A. J., Holbrook, N. J., Perkins-Kirkpatrick, S. E., Scannell, H. A., Straub, S. C., & Wernberg, T. (2018). Longer and more frequent marine heatwaves over the past century. *Nature Communications*, 9(1). <https://doi.org/10.1038/s41467-018-03732-9>

- Park, J., Lee, H., De Saeger, J., Depuydt, S., Asselman, J., Janssen, C., Heynderickx, P. M., Wu, D., Ronsse, F., Tack, F. M. G., Hiraoka, M., Pandey, L. K., Mašek, O., Hung, Y., & Han, T. (2024). Harnessing green tide *Ulva* biomass for carbon dioxide sequestration. *Reviews in Environmental Science and Bio/Technology*. <https://doi.org/10.1007/s11157-024-09705-3>
- Pastor, F., Valiente, J. A., & Palau, J. L. (2019). Sea surface temperature in the Mediterranean: Trends and spatial Patterns (1982–2016). In *Pageoph topical volumes* (pp. 297–309). https://doi.org/10.1007/978-3-030-11958-4_18
- Predation rates on juvenile blue crabs in estuarine nursery habitats: evidence for the importance of macroalgae (*Ulva lactuca*) on JSTOR. (n.d.). www.jstor.org. <http://www.jstor.org/stable/24842199>
- Rahhou, A., Layachi, M., Akodad, M., Ouamari, N. E., Rezzoum, N. E., Skalli, A., Oudra, B., Bakali, M. E., Kolar, M., Imperl, J., Petrova, P., Moumen, A., & Baghour, M. (2023). The Bioremediation Potential of *Ulva lactuca* (Chlorophyta) Causing Green Tide in Marchica Lagoon (NE Morocco, Mediterranean Sea): Biomass, Heavy Metals, and Health Risk Assessment. *Water*, 15(7), 1310. <https://doi.org/10.3390/w15071310>
- Ribeiro, J., Bentes, L., Coelho, R., Gonçalves, J. M., Lino, P. G., Monteiro, P., & Erzini, K. (2006). Seasonal, tidal and diurnal changes in fish assemblages in the Ria Formosa lagoon (Portugal). *Estuarine Coastal and Shelf Science*, 67(3), 461–474. <https://doi.org/10.1016/j.ecss.2005.11.036>
- Roleda, M. Y., & Heesch, S. (2021). Chemical profiling of *Ulva* species for food applications: What is in a name? *Food Chemistry*, 361, 130084. <https://doi.org/10.1016/j.foodchem.2021.130084>
- Sampath-Wiley, P., Neefus, C. D., & Jahnke, L. S. (2008). Seasonal effects of sun exposure and emersion on intertidal seaweed physiology: Fluctuations in antioxidant contents, photosynthetic pigments and photosynthetic efficiency in the red alga *Porphyra umbilicalis* Kützing (Rhodophyta, Bangiales). *Journal of Experimental Marine Biology and Ecology*, 361(2), 83–91. <https://doi.org/10.1016/j.jembe.2008.05.001>
- Scheffer, M., & Carpenter, S. R. (2003). Catastrophic regime shifts in ecosystems: linking theory to observation. *Trends in Ecology & Evolution*, 18(12), 648–656. <https://doi.org/10.1016/j.tree.2003.09.002>
- Shahar, B., & Guttman, L. (2020). An integrated, two-step biofiltration system with *Ulva fasciata* for sequenced removal of ammonia and nitrate in mariculture effluents. *Algal Research*, 52, 102120. <https://doi.org/10.1016/j.algal.2020.102120>
- Short, J., Foster, T., Falter, J., Kendrick, G. A., & McCulloch, M. T. (2015). Crustose coralline algal growth, calcification and mortality following a marine heatwave in Western Australia. *Continental Shelf Research*, 106, 38–44. <https://doi.org/10.1016/j.csr.2015.07.003>

- Simon, C., McHale, M., & Sulpice, R. (2022). Applications of *Ulva* biomass and strategies to improve its yield and composition: A Perspective for *Ulva* Aquaculture. *Biology*, *11*(11), 1593. <https://doi.org/10.3390/biology11111593>
- Smetacek, V., & Zingone, A. (2013). Green and golden seaweed tides on the rise. *Nature*, *504*(7478), 84–88. <https://doi.org/10.1038/nature12860>
- Soares, M. O., Rabelo, E. F., & Gurgel, A. L. (2023). Marine heatwaves lead to bleaching and mass mortality in a key zoantharian. *Marine Biodiversity*, *53*(1). <https://doi.org/10.1007/s12526-022-01319-8>
- Stahl, W., & Sies, H. (2003). Antioxidant activity of carotenoids. *Molecular Aspects of Medicine*, *24*(6), 345–351. [https://doi.org/10.1016/s0098-2997\(03\)00030-x](https://doi.org/10.1016/s0098-2997(03)00030-x)
- Walls, A., Edwards, M., Firth, L., & Johnson, M. (2018). Ecological priming of artificial aquaculture structures: kelp farms as an example. *Journal of the Marine Biological Association of the United Kingdom*, *99*(4), 729–740. <https://doi.org/10.1017/s0025315418000723>
- Wang, S., Jing, Z., Wu, L., Sun, S., Peng, Q., Wang, H., Zhang, Y., & Shi, J. (2023). Southern hemisphere eastern boundary upwelling systems emerging as future marine heatwave hotspots under greenhouse warming. *Nature Communications*, *14*(1). <https://doi.org/10.1038/s41467-022-35666-8>
- Wang, X., Liu, F., & Jiang, D. (2017). Priming: A promising strategy for crop production in response to future climate. *Journal of Integrative Agriculture*, *16*(12), 2709–2716. [https://doi.org/10.1016/s2095-3119\(17\)61786-6](https://doi.org/10.1016/s2095-3119(17)61786-6)
- Wernberg, T., Bennett, S., Babcock, R. C., De Bettignies, T., Cure, K., Depczynski, M., Dufois, F., Fromont, J., Fulton, C. J., Hovey, R. K., Harvey, E. S., Holmes, T. H., Kendrick, G. A., Radford, B., Santana-Garcon, J., Saunders, B. J., Smale, D. A., Thomsen, M. S., Tuckett, C. A., . . . Wilson, S. (2016). Climate-driven regime shift of a temperate marine ecosystem. *Science*, *353*(6295), 169–172. <https://doi.org/10.1126/science.aad8745>
- Wichard, T., Charrier, B., Mineur, F., Bothwell, J. H., De Clerck, O., & Coates, J. C. (2015). The green seaweed *Ulva*: a model system to study morphogenesis. *Frontiers in Plant Science*, *6*. <https://doi.org/10.3389/fpls.2015.00072>
- Yang, J. J., Yu, D. C., Feng, Y., MA, Yin, Y., & Shen, S. D. (2019). Antioxidative defense response of *Ulva prolifera* under high or low-temperature stimulus. *Algal Research*, *44*, 101703. <https://doi.org/10.1016/j.algal.2019.101703>

- Yong-Ling, Ruan, Ye, Jin, Yue-Jian, Yang, Guo-Jing, Li, John, & Boyer. (2010). Sugar input, metabolism, and signaling mediated by invertase: roles in development, yield potential, and response to drought and heat. *分子植物 : 英文版*, 6, 942–955.
<http://www.cqvip.com/QK/90143B/201006/36457525.html>
- Zanolla, M., Carmona, R., Kawai, H., Stengel, D. B., & Altamirano, M. (2019). Role of thermal photosynthetic plasticity in the dispersal and settlement of two global green tide formers: *Ulva pertusa* and *U. ohnoi*. *Marine Biology*, 166(10). <https://doi.org/10.1007/s00227-019-3578-1>
- Zheng, M., Lin, J., Zhou, S., Zhong, J., Li, Y., & Xu, N. (2019). Salinity mediates the effects of nitrogen enrichment on the growth, photosynthesis, and biochemical composition of *Ulva prolifera*. *Environmental Science and Pollution Research*, 26(19), 19982–19990. <https://doi.org/10.1007/s11356-019-05364-y>
- Zou, D., & Gao, K. (2014a). The photosynthetic and respiratory responses to temperature and nitrogen supply in the marine green macroalga *Ulva conglobata* (Chlorophyta). *Phycologia*, 53(1), 86–94. <https://doi.org/10.2216/13-189.1>
- Zou, D., & Gao, K. (2014b). The photosynthetic and respiratory responses to temperature and nitrogen supply in the marine green macroalga *Ulva conglobata* (Chlorophyta). *Phycologia*, 53(1), 86–94. <https://doi.org/10.2216/13-189.1>

Ringraziamenti

Voglio ringraziare di cuore la professoressa Isabella Moro per il grande aiuto e il sostegno continuo durante questo percorso.

Un grazie speciale anche al professor Marco Munari, a Ilaria e a tutti i membri dell'ufficio per il supporto nelle analisi statistiche e la loro disponibilità.

Grazie ai professori Joao Da Silva e Isabel Barrote per avermi dato l'opportunità di svolgere il tirocinio nel loro laboratorio in Portogallo, un'esperienza che porterò sempre con me.

Un ringraziamento va anche ai miei amici, che hanno reso più leggeri i momenti difficili e con cui ho creato tutti i ricordi più belli di questa avventura.

Infine, grazie alla mia famiglia, che ha sopportato tutti i miei "non ce la posso fare" e mi ha incoraggiata e sostenuta lungo tutto il percorso.

Senza di voi non sarebbe stato possibile arrivare fino a qui!